Alterations of plastics spectra in MIR and the potential impacts on identification towards recycling

Charles Signoret, Anne-Sophie Caro-Bretelle, José-Marie Lopez-Cuesta, Patrick Ienny, Perrin Didier

Alterations of plastics spectra in MIR and the potential impacts on identification towards recycling

Charles Signoret[a], Anne-Sophie Caro-Bretelle[b], José-Marie Lopez-Cuesta[a], Patrick Ienny[b], Didier Perrin[a,*]

[a] Polymers Composites and Hybrids (PCH), IMT Mines Ales, Ales, France
[b] LMGC, IMT Mines Ales, Univ. Montpellier, CNRS, Ales, France

A B S T R A C T

Plastic recycling is mainly limited by their sorting as their natures, forms and formulation are very numerous and most of them are strongly incompatible, leading to poor mechanical properties. Several industrial sorting technologies exist, and others are in development. However, each of them has drawbacks. Especially, NIR-HSI (Near-Infrared Hyperspectral Imagery) is limited by the use of carbon black, mainly as a pigment and UV agent in the case of thermoplastics. MIR-HSI (Mid-Infrared) could be a suitable and viable alternative to resolve this issue. Hence, this work, based on laboratory FTIR-ATR (Fourier-Transform Infrared Attenuated Total Reflection), focuses on possible sources of spectral alteration, which could impair identification of usual polymers using industrial MIR-HSI. It aims to help simple and rapid laboratory characterization and give tools to avoid mis-identification or enable specific segregation during industrial sorting. First, acquisition parameters were de-graded to simulate those imposed by industrial conditions: short acquisition time, diminished resolution and blank defaults. Then, impact on formulations of usual WEEE (Waste of Electric and Electrical Equipment) plastics were evaluated, with PE, PP, ABS and HIPS as matrices, and carbon black (at different concentrations), calcite, talc, titanium oxide and some flame retardants as additives. Several patterns found in homemade standard samples were recognized within a stock of about one hundred of real waste samples.

Keywords:
Polymer recycling
Sorting
MIR
WEEE
Identification
Formulated plastics

1. Introduction

Plastic recycling is viewed as one of the most interesting ways to deal with environmental problems linked to both their production and disposal (Wäger and Hischier, 2015; WRAP, 2008). Nevertheless, reaching interesting properties, as processability, aspect or mechanical performance, is very difficult to achieve as plastics natures, additives, fillers, forms and applications are incredibly diverse. Most of them are non-miscible and even incompatible (Maris et al., 2018), since their blends display functional properties inferior to each of them taken separately. An efficient and accurate sorting of end-of-life plastics is thus primordial for recycling to be economically pertinent (Vrancken et al., 2017). However, end-of-life management itself also entails ecological impacts. For instance, these plastics needs to be cleaned and thus need water and sometimes detergents. Also, collection and, transport can also bear a severe carbon footprint, especially if these actions are geographically scattered (WRAP, 2008).

Several types of separation technologies exist. They can be classified in two different groups: direct and indirect (Gundupalli et al., 2017). When separation is intrinsically due to property differences, it is direct.

Abbreviations & acronyms: ABS, Acrylonitrile Butadiene Styrene; APP, Ammonium Polyphosphate; ATR, Attenuated Total Reflection; $CaCO_3$, Calcium carbonate or calcite (chalk); CB, Carbon Black; DSC, Differential Scanning Calorimetry; FR, Flame Retardant; FTIR, Fourier Transform Infrared; HBCD, Hexabromocyclododecane; HDPE, High Density Polyethylene; HIPS, High Impact Polystyrene; HSI, Hyperspectral Imagery; LIBS or LIPS, Laser Induced Breakdown/Plasma Spectroscopy; LWIR, Long Wavelength Infrared (7.4-14.0 μm or 1350-700 cm^{-1}); MIR, Mid-Infrared (4000-400 cm^{-1} or 2.5-25.0 μm); MWIR, Middle Wavelength Infrared - 2 to 5 μm (5000 to 2000 cm^{-1}); NIR, Near-Infrared – 0,8 to 2,5 μm (12500 to 4000 cm^{-1}); PC, Polycarbonate (from bisphenol A); PE, Polyethylene; PMMA, Polymethylmethacrylate; PP, Polypropylene; PPC or PP copo, Polypropylene copolymer; PPH or PP homo, Polypropylene homopolymer; PVC, Polyvinyl chloride; PS, Polystyrene; RoHS, Regulation of Hazardous Substances; SEM/EDX, Scanning Electron Microscopy / Energy Dispersive X-ray spectroscopy; Sb_2O_3, Antimony (tri) oxide; SNR, Signal-to-Noise Ratio; TBBPA, Tetrabromobisphenol A; TGA, Thermogravimetric analysis; THz, Terahertz; WEEE or W3E, Waste of Electrical & Electronic Equipment

* Corresponding author.
E-mail address: didier.perrin@mines-ales.fr (D. Perrin).

It is the case with sink-float tanks (Gent et al., 2009) where sorting is based on density differences. Other examples are froth flotation for surface tension (Wang et al., 2015), trommels for granulometry (Ashkiki et al., 2019), magnetic overhead belts and Eddy current for (para)magnetic properties (Krivtsova et al., 2009). Sorting is indirect when identification and separation are performed through two different steps (Gundupalli et al., 2017). Generally, these are optical technologies. Items to be sorted are moved on a conveyor belt where a sensor acquires their spectral signature after adequate excitation. Then, these items are physically sorted, usually through the use of compressed air nozzles.

The transposition to industrial dynamical conditions of several static technologies, used at laboratory scale, such as UV-Vis (Gundupalli et al., 2017), NIR (Near-Infrared) (Beigbeder et al., 2013; Huth-Fehre et al., 1995; Leitner et al., 2003), MIR (Mid-Infrared) (Bae et al., 2019; Becker et al., 2017; Rozenstein et al., 2017), Raman spectroscopies (Bae et al., 2019; Florestan et al., 1994; Roh et al., 2017), LIBS (Laser Induced Breakdown Spectroscopy) (Barbier et al., 2013; Grégoire et al., 2011), X-ray transmission or fluorescence (Hasan et al., 2011; Mesina et al., 2007) is currently studied. Laboratory analysis generally explores a single sample at a time, on a relatively small spot, can take from several seconds to hours, can be sometimes made with contact to the sample. However, industrial identification toward waste sorting is radically different. Objects are generally scattered along a high-speed conveyor belt and their identification must be made remotely within milliseconds to enable sorting at the end of the conveyor. This leads to strong technological differences, which, with the harsh acquisition conditions, often lead to difficult-to-analyze signals. Available data, spatial and spectral resolutions, signal-to-noise ratio (SNR) can be, at first glance, insufficient to enable identification. This requires signal processing and use of advanced classification algorithms (Roh et al., 2017; Spetale et al., 2016; Tachwali et al., 2007; van den Broek et al., 1998). However, a real physicochemical understanding of the differences at the source of classification is needed to avoid false identifications.

Additives and fillers can also have repercussions on sorting. As polyolefins are the main polymers with intrinsic densities below 1 g/cm^3, they can be recovered thanks to tap water sink-float. Sadly, an important fraction is filled with calcite (calcium carbonate, $CaCO_3$) or talc (Aluminum Silicate, $Al_2Si_2O_5(OH)_4$) and thus sinks (Maris et al., 2015). Peeters et al. (Peeters et al., 2014) highlighted density overlapping because of the use of flame retardants and styrenic blends, making density separation inefficient. In the frame of WEEE (Waste Electrical and Electronic Equipment) legislation and RoHS (Regulation of Hazardous Substances), numerous widely spread halogenated flame retardants (FR) are now forbidden because of their toxicity. Several other widely used FRs could also become forbidden in the future (Delva et al., 2018; Vilaplana et al., 2008). This imposes sorting materials according to these additives for recycled materials to stay below legal thresholds (Hennebert and Filella, 2018). X-ray transmission and fluorescence are among the most promising technologies towards this goal (Gallen et al., 2014; Kuang et al., 2018; Sharkey et al., 2018). Even in a dual energy configuration, which is well developed and perfectly suitable to metals (Mesina et al., 2007), transmission lacks selectivity between heavy elements. In the case of additive plastics, both concentration and thickness are unknowns in the Beer-Lambert law whereas concentration was assumed 100% in the case of metals. As it needs to detect way more wavelengths, fluorescence is technologically more challenging and thus more expensive. Solvent extraction of FRs or total dissolution could be very efficient (Grause et al., 2015; Vilaplana et al., 2009; Zhao et al., 2018), although transposition to industrial scale can be difficult, especially with solvent management. Pyrolysis, towards energy recovery and/or chemical recycling (Ma et al., 2016; Yang et al., 2013) could be seen as the only viable solution, even if rather controlled waste stocks (thus sorted) are needed not to disrupt the process and its efficiency too much. Even at laboratory scale, precise identification and quantification of flame retardants can be rather burdensome compared to simple infrared spectra, especially with the need of appropriate extraction (Guzzonato et al., 2016a; Otake et al., 2015; Schlummer et al., 2005; Vilaplana et al., 2008). However, Puype et al. (Puype et al., 2019) recently showed that Direct Analysis in Real Time - High Resolution Mass Spectrometry (DART-HRMS) was adequate to rapidly and accurately identify brominated FR at laboratory scale.

Another very common additive, carbon black, which is the most common way to color plastic in black or grey, strongly absorbs in NIR (Beigbeder et al., 2013; Huth-Fehre et al., 1995; Serranti et al., 2012), making NIR-HSI unable to sort dark colored plastics. Its absorption is easily explained by the almost infinite unsaturations conjugation within its graphitic structure (Kang et al., 2016), also explaining its deep black color as it absorbs in the visible range. It also absorbs beyond these boundaries in NIR but also in UV (Allen et al., 1998; Liu and Horrocks, 2002), making it an interesting additive to protect polymeric materials from photodegradation. Consequently, it also impacts Raman spectra more or less depending on the excitation wavelength (Bokobza et al., 2013; Yamaji et al., 2013). More generally, carbon black is used for coloration and UV protection from 0.5 to 2.0 wt. % (Turner, 2018), up to 20 wt. % for electrical conductivity where percolation is necessary (Probst et al., 2009; Zhou et al., 2006) and up to 50 wt. % for mechanical reinforcement (Kang et al., 2016; Li et al., 2019), especially in elastomers as in tires. As NIR-HSI, the most used technology to finely discriminate plastics according to their natures, is limited with dark plastics, several alternative sorting technologies are subject to extensive research (Grégoire et al., 2011; Huang et al., 2017; Küter et al., 2018; Langhals et al., 2014; Roh et al., 2017; Wang et al., 2015; Zhao et al., 2018; Zhao et al., 2018). MIR-HSI is one of them (Kassouf et al., 2014; Rozenstein et al., 2017; Signoret et al., 2019a, 2019b). It was chosen in the present study because this technology begins to be commercially available. Also, Fourier-Transform Infrared (FTIR), its laboratory equivalent as it works within the MIR range, was used for a long time for polymer analysis.

The present study aims to complete our previous works on spectral identification of polymers through the use of FTIR-ATR (Attenuated Total Reflection) with the scope of transposition to MIR-HSI. The first study described intrinsic signals of styrenics polymers and their blends (Signoret et al., 2019a). The second one focused on polyolefins and polymers with close spectra, namely PVC and POM (Signoret et al., 2019b). A third one was about spectral alterations due to ageing of LDPE, PPH, HIPS, ABS and PC in the scope of their identification (Signoret et al., 2020). Whereas these previous works focused on characteristic signals of polymers, the subject here is to anticipate how these patterns can evolve because of formulation: carbon black, common mineral fillers and flame retardants. The objective is to determine if loaded polymers could still be recognizable, even in degraded acquisition conditions. Also, characteristic patterns related to formulation can be useful to quickly identify additives, at least at laboratory scale, instead of using a heavier technique as ICP (Inductively Coupled Plasma) or X-ray fluorescence which can be more time and money consuming. However, accurate quantification needs another technique, namely thermogravimetric analysis (TGA).

2. Materials and methods

2.1. Materials

Several polymers were used for formulated standard preparation: ABS reference was Terluran GP22 (Styrolution), HIPS was Polystyrol 485I (Repsol), ABS/PC was Bayblend T85 XF (Covestro), PE was HDPE Alcudia 4810 (Sabic), PP was PPC 83MF10 and PPH 505P (Sabic). Carbon black used in this study was Elftex 570 (Cabot). Several mineral fillers references were also involved: XP12-5630 kaolin (IMERYS), Omya BL calcite (Omya), Luzenac HAR T84 talc (IMERYS) and

Table 1
Specific signals of some mineral fillers and atmospheric species specific signals – from pale yellow to red to qualify relative intensity

	Wavenumbers (cm^{-1})														
Species	1400	1300	1120	1100	1030	1015	910	885	870	790	760	750	710	690	670
Talcum				peak at 1010							761				670
Kaolin			1114		1032	1008	914			791		754		696	
$CaCO_3$	peak at 1406								873				712		
TiO_2								877		peak at 650, shoulder at 570-540					
CO_2															670
H_2O	Noise-like														

Aeroxide TiO_2 P 25 titanium dioxide (Evonik). Some flame retardants (FR) were used as received to prepare standard blends: ammonium polyphosphate (APP Exolit AP 423 (Clariant), Dechlorane C25+ (ABCR) and TBBPA reference 330396 from Sigma-Aldrich. Two other FRs were analyzed in powder form because of insufficient available amounts: antimony (tri) oxide (Sb_2O_3) was Empura (Merck), and HBCD (1,2,5,6,9,10-hexabromocyclododecane) was the SI-21691 analytical standard provided by Analytical Lab (France). The 112 waste samples were kindly provided by the Suez company from their plants in Feyzin (SUEZ RV DEEE) and Berville-sur-Seine (NORVAL) in France, mainly from WEEE but also from municipal deposits. About two third of them were dark-colored.

2.2. Formulated standards preparation

For ABS, HIPS and ABS/PC transformation, materials were dried at least 16 hours at 80°C before transformation. For large quantity formulation campaigns, of the order of kilograms, masterbatches were realized in a Rheomix 3000 internal mixer (Haake). Masterbatches were then diluted with a Clextral 900 BC21 twin screw extruder (Clextral). For small quantity formulation campaigns, of the order of tens to a hundred grams, a DSM MC40 microextruder (Xplore) was used. Masterbatches were made then diluted twice to four times depending on the desired concentration. The minimum of two-step was chosen to ensure concentration homogeneity as first mixes are often heterogeneous, especially in internal mixer. All materials were processed between 210 and230°C. For spectral characterization, especially in FTIR-ATR, standard samples were produced in the form of disks with 25 mm diameter and 1.5 mm thickness. A Zamak-Mercator injection molding machine was used in this purpose.

2.3. Thermogravimetric analysis

A Pyris 1 TGA provided by Perkin-Elmer was used to estimate carbon black loadings within real waste samples and produced standards. Temperature was raised from 30°C to 900°C at 10°C/min. Samples were analyzed under nitrogen at 20 mL/min up to 650°C, where most of polymeric parts are degraded, then under air at same flow where carbon black degrades. At least, three measures were averaged for each batch. Curve examples are given in appendix A. It can be seen that virgin samples are not totally degraded before after the gas switch. Thus, the ≈1.8 wt. % loss attributed to ABS must be subtracted from the carbon black rate. Additionally, the final mass is subjected to tare imprecision and losses below 200°C can be associated to volatiles, especially humidity. Thus, the carbon black loading rate τ_{NC} (wt. %) is calculated as follows from mass losses $\Delta m(\Delta T)_X$ (wt. %) where ΔT (°C) corresponds to temperature ranges and X refers to samples or references:

$$\tau_{NC} = \frac{\Delta m(650 - 900\,°C)_{sample} - \frac{\Delta m(650-900\,°C)_{ref} \times \Delta m(200-650\,°C)_{sample}}{\Delta m(200-900\,°C)_{ref}}}{\Delta m(200 - 900\,°C)_{sample}}$$

2.4. FTIR Spectroscopy

A Vertex 70 FT MIR spectrometer from Bruker with an ATR unit equipped with a diamond crystal was used. Unless indicated otherwise, resolution was at 4 cm^{-1}, 16 scans for background acquisition and 16 scans for the sample spectrum. Most of the samples were directly analyzed on the crystal. Some were cut to obtain better acquisition as ATR is sensitive to surface aspects. Analyzed surfaces were cleaned with ethanol and left to dry. Spectra were acquired from 4000 to 400 cm^{-1} and analyzed thanks to the OPUS software provided with the spectrometer. Matlab 2018 and Origin 9 were also used for further processing. FTIR-ATR (Attenuated Total Reflection) was chosen for convenience and to be closer to HSI cameras as both are reflective technologies. For carbon black powder analysis, a transmission unit was used on KBr (potassium bromide) disks at a 4 cm^{-1} resolution, 32 scans for background and for sample.

2.5. SEM/EDX: Scanning electron microscopy – Energy dispersive X-ray spectroscopy

SEM analysis was performed with a Quanta 200 FEG from Thermo Fischer Scientific on waste samples. The use of an Oxford energy-dispersive X-ray spectroscopy (EDX) sensor allowed to carry out elemental imaging of samples.

2.6. Spectra comparison methodology description

The overall methodology of this work is based on the use of charts as Table 1. It gathers every encountered within 10 cm^{-1} wide columns. Other charts are available in *supporting information*, covering both MWIR and LWIR, and every polymer described in previous works. The applied colors relate the visually relative intensities of the corresponding signal within the considered range, similarly with the "strong" or "weak" mentions frequently found in correlation tables. Purple, red, orange, yellow and light yellow respectively correspond to "very strong", "strong", "medium" "weak" and "very weak". Blue is used for signals highly variable in intensity. These charts are useful as signals and specific patterns of a chemical species or a family are highlighted by columns empty elsewhere. Also, they can be used in the other way when looking for an unknown encountered peak. However, one should pay attention to complementary signals, as an isolated peak can correspond to several species.

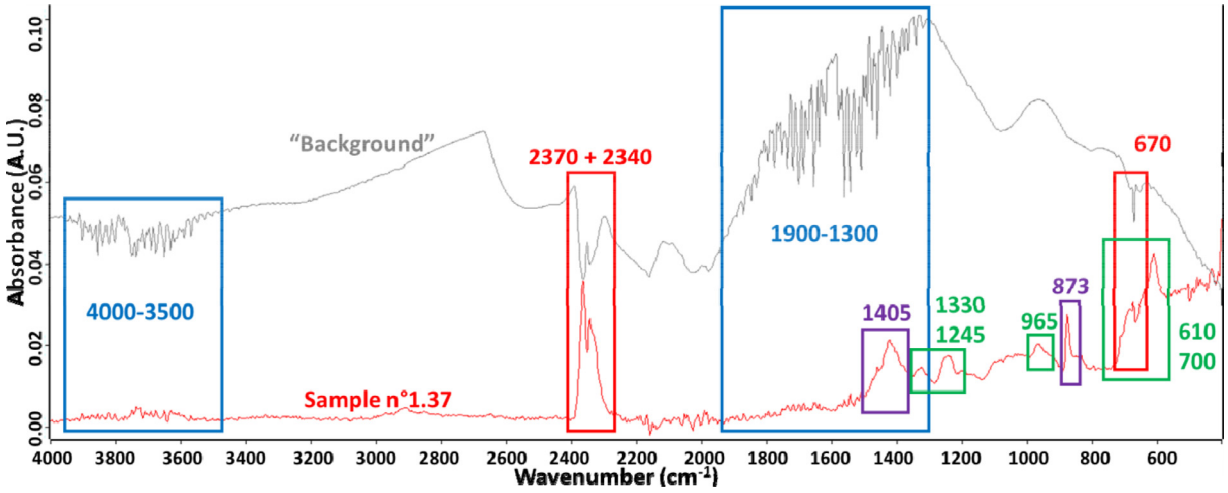

Figure 1. Pathologic FTIR-ATR spectrum of waste sample n°1.37 & corresponding background spectrum - signals of CO_2 framed in red, H_2O in blue, PVC in green and calcite in purple

3. Results and discussion

3.1. Degraded acquisition

3.1.1. Background/blank default: Atmospheric IR absorbent species - CO_2 & H_2O

CO_2 and H_2O are more and more visible as background/blank is too old compared to current acquisition and as intrinsic signals from the polymer are weak as seen on Fig. 1. As all analyzed surfaces were first cleaned with ethanol and left to dry, observed water signals are probably corresponding to atmospheric water. The polymer corresponding to this spectrum can still be identified as calcite loaded PVC. Calcite specific signals are described in Part 3.3. PVC is mainly identified through its 700 and 610 cm^{-1} pattern characteristic of C-Cl stretching (Signoret et al., 2019b). H_2O signals, seen from 4000 to 3500 cm^{-1} for MWIR, and 1900 to 1300 in MIR, framed in blue on Fig. 1, could be perceived as noise but its particular pattern is characteristic of several gaseous species, preventing confusion with plastics. Whereas rotational levels are strained in condensed phases by surrounding molecules, they are "pure" in gas phase, each gap between observed lines corresponding to a distinct excitation level, explaining their regularity and respective heights (Hollas, 2004). Other atmospheric species as nitrogen or oxygen cannot absorb in infrared as asymmetry cannot be introduced in their dipole moment with bending (Hollas, 2004). However, they can in Raman as excitation mode is different (Fletcher and Rayside, 1974) and this could strongly disrupt industrial applications.

Way more pronounced than H_2O, CO_2 has two very famous bands at 2370 and 2340 cm^{-1} in MWIR. Excluding isocyanate (N=C=O) stretching at 2270 cm^{-1} which can be residually found in some polyurethanes, and nitrile (C≡N) stretching at 2237 cm^{-1} for ABS or SAN, no specific polymer signals were found from 2000 to 2500 cm^{-1} (MWIR chart in *supporting information*). Thus, this signal should not mask important peaks. In LWIR, CO_2 has a very thin peak at 670 cm^{-1} (Hossain et al., 2014). Within 10 cm^{-1}, as seen in the LWIR chart in *supporting information*, calcite, TBBPA and Dechlorane have a peak here, but being larger for the first one, and accompanied by many other peaks for the two others, as described further below. Checking complementary signals rapidly eliminates any doubt.

Atmospheric species should moderately impact polymer industrial identification as concerned ranges do not overlap each other or signal nature is different (as with atmospheric water). It is thus important to consider them separately in a classifier learning phase, not to include atmospheric parameters in plastic identification, as they can be hardly controllable at reasonable costs. Also, they can represent a numerical "dead weight", inducing useless data treatment.

3.1.2. Short acquisition time: diminishing number of scans in FTIR

Figure 2.a) shows the spectral evolution by diminishing the number of scans in FTIR-ATR on an ABS standard. Both sensor noise and "atmospheric noise" are amplified with reduction of scans. In this particular case, it does not challenge identification as the polymer signal was strong. In industrial conditions, acquisition time is very short for material throughput reasons but several pixels are acquired for each object, mimicking plural scans. It can however be expected that Signal-to-Noise Ratios (SNR) should be far lower.

3.1.3. Evolution with resolution

Figure 2.b) shows the impact of resolution refinement on a PP reference MIR spectrum. A strongly defined spectrum tends to display stronger noise, especially here, where only one scan was performed for each spectrum. Again, atmospheric species are fostered. Thus, resolution and acquisition time must be tuned altogether. With degraded resolution, peaks get convoluted and weaker, as they tend to be partially averaged with baseline. Especially here, the four distinct peaks of PP (C-H stretching) between 2800 and 3000 cm^{-1} merge into a single shape (blue frame in Fig. 2.b)). It happens even more rapidly with CH_3 C-H bending at 1375 cm^{-1} (purple frame and magnification) where the presence of shoulder underlines crystallinity (Signoret et al., 2019b). It is evident that convolution intervene faster as peaks are close and weak. Noise can appear milder at 4 cm^{-1} resolution than on its equivalent on Fig. 2.a) but it is probably mainly due to scaling and numerical offsets different which were differently chosen here to highlight convolution of signals. Finally, the black framed magnification of Fig. 2.b) shows how a weak signal disappears as it is averaged with the baseline. It is the example of the 2725 cm^{-1} peak, very specific to PP as it is alone within its column in the MWIR chart (*supporting information*). Combined with rather weak signals due to short acquisition time, this can lead to important information loss, detrimental to fast identification.

3.1.4. Conclusions on degraded acquisition

Atmospheric species can display important signals but are located in specific zones and should not negatively impact polymer identification if well taken in account. Short acquisition time mainly impacts signal-to-noise ratio whose degradation can be tempered with radiation source intensity. However, this can lead to serious heating. The depreciation of resolution leads to the convolution of peaks and global reduction of intensities, which can lead to the visual disappearance of small peaks.

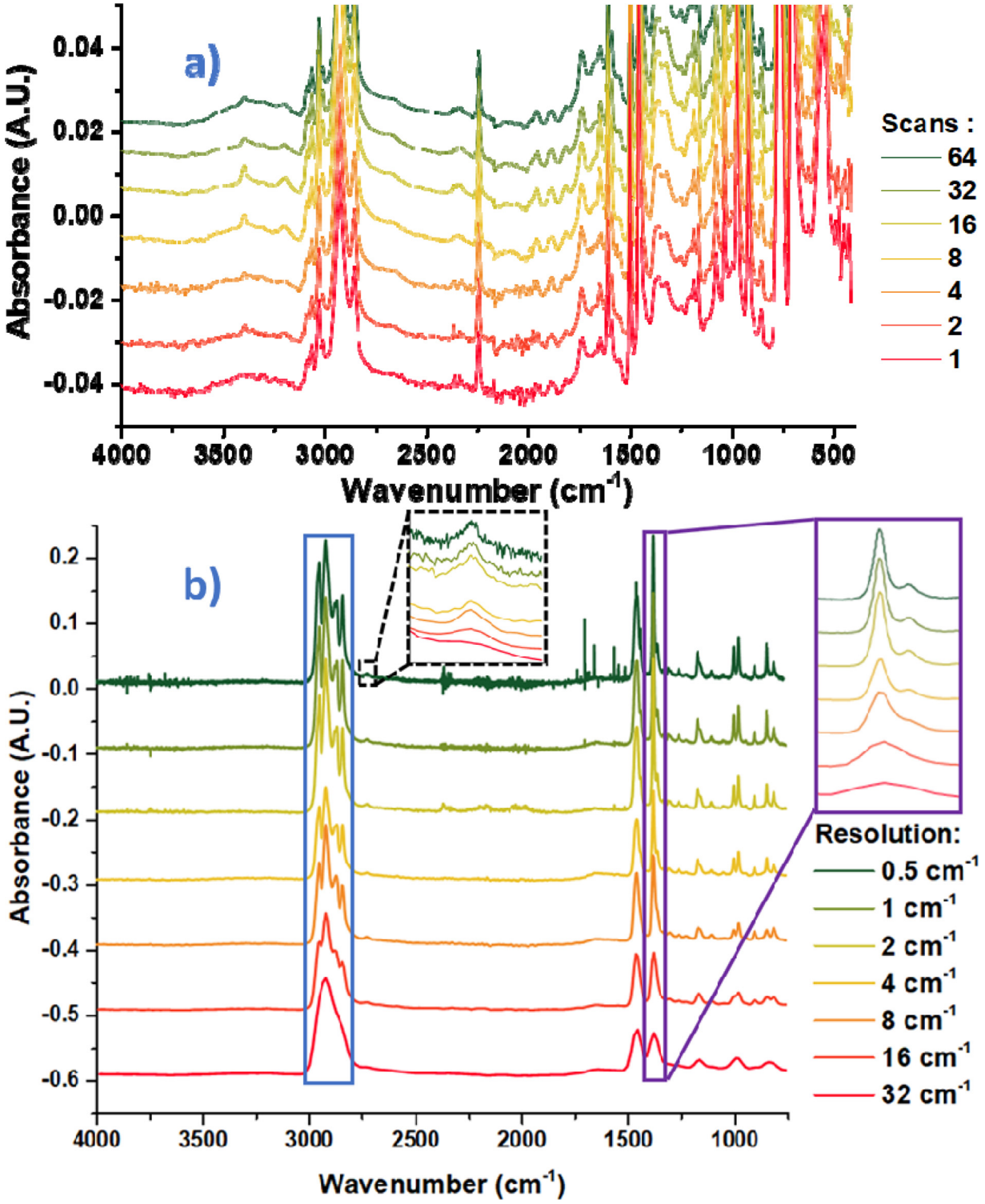

Figure 2. Impacts of acquisition parameters in FTIR-ATR on the quality of spectra: a) Number of scans reduction on an ABS standard with a 4 cm^{-1} resolution b) Resolution degradation on a PP standard with 1 scan per measure – blue frame for C-H stretching convoluting signals and purple for crystallinity marker

3.2. Carbon black impact on MIR spectra

As carbon black strongly absorbs in UV, in the visible range and in NIR, one could worry about its absorption in MIR and possible induced disturbances in polymer identification. In the purpose to qualify this impact, carbon black powder and homemade dark colored samples were characterized in FTIR-ATR.

3.2.1. Carbon black-KBr disks in FTIR-Transmission

To avoid spectral defects from ATR, which distorts baselines as infrared penetration depends on its wavenumber, carbon black was analyzed in transmission after dilutions within dried KBr. Fig. 3 shows spectra obtained with 1.00 and 0.25 wt. % disks which were equally totally black to the naked eye. At 1.00 wt. %, transmission is at 0% on the whole range and the absorbance curve highlights the sensor's limit of sensitivity. At 0.25 wt. %, transmission is below 2% on most of the

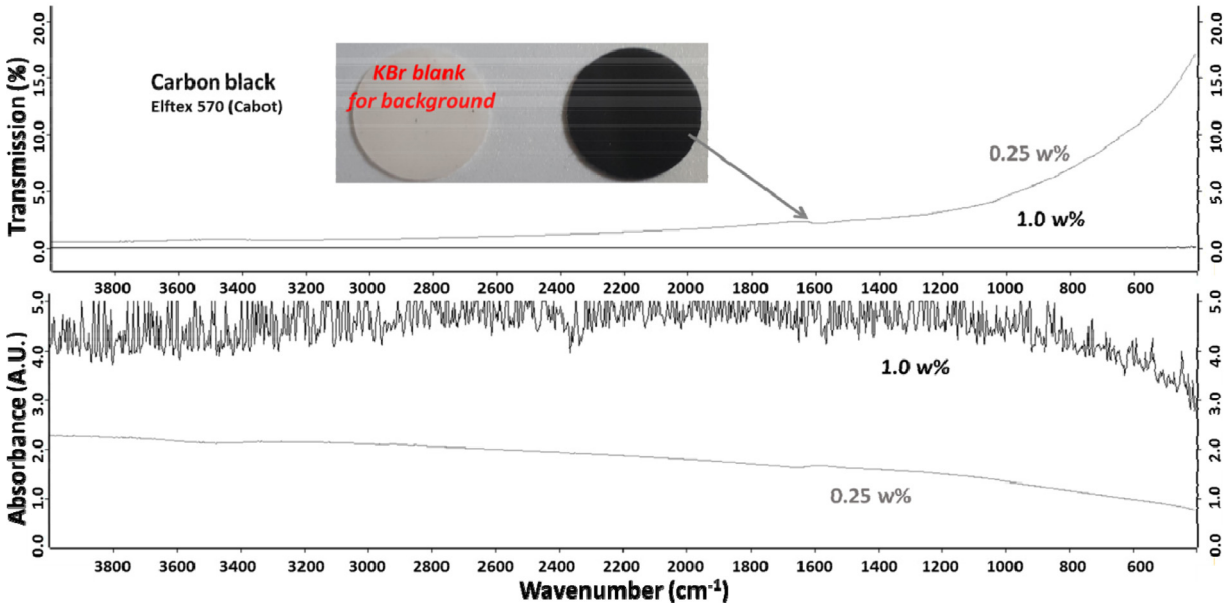

Figure 3. FTIR spectra in transmission of carbon black in KBr disks, no normalization or numerical offset – picture of pure KBr and 0.25 wt. % carbon black KBr disks

range and rapidly rises up to 20% on the last 1000 cm^{-1}. Logically, absorbance slightly and steadily decreases from 2000 to 400 cm^{-1}, from 2 to 1 A.U. It appears that a higher carbon black content leads to a higher absorbance baseline (and lower transmission baseline).

No special features, as C-H, O-H or C=O marks, can be observed, meaning that the graphitic structure is rather predominant and material is not visibly oxidized. As the graphitic sheets are semi-infinite and thus double bonds highly conjugated, absorption seems continuous from UV up to MIR.

3.2.2. 2 wt. % loaded PE, PP, HIPS & ABS samples

PE, PP, HIPS and ABS spectroscopic standards were made and controlled by TGA at 2 wt. % carbon black. This concentration was chosen as it is the most current loading rate for coloring thermoplastics and for protecting them from photodegradation. As specified previously, higher rates are applied for elastomers reinforcement, or electrical conductivity, which are both scarce among WEEE. Fig. 4 was produced without numerical offsets of the curves and by repeating each measure four times on different specimens or spots. The resolution was 4 cm^{-1} and acquisition was made in 16 scans. Same parameters are applied for all data given from this point. The most important feature is a shift of absorbance baseline, more or less important depending on the polymer, but generally of about 0.01 to 0.02 A.U. It is coherent with spectra of carbon black alone in KBr, as it is a continuous absorption. Interestingly enough, HIPS and ABS baselines were already above 0 U.A., at about 0.04 U.A. at 4000 cm^{-1} and at about 0.07 U.A. at 400 cm^{-1}, highlighting the ATR defect. This defect, intrinsic to ATR, fosters stronger absorption at lower wavenumbers because infrared penetration within the sample depends on its wavenumber. This defect is also more or less intense depending on the quality of acquisition, mainly due to the surface-crystal contact.

Even though carbon black intrinsically absorbs less at low wavenumbers, its presence seems to amplify this defect as the shift is of only 0.01 U.A. on the left side and up to 0.06 U.A. on the right side. This can be explained as infrared rays penetration is affected by the presence of carbon black. Effects on polymer peaks intensity seem negligible in this concentration range. Identification through MIR seems unaffected for these polymers at these loading rates.

3.2.3. ABS at different carbon black loading rates between 0.05 & 4.50 wt. %

To study further the impact of carbon black on MIR spectral features, several ABS standards were made at different loading rates of carbon black. Always under TGA control, a first series from 0.5 to 2.0 wt. % was made in extrusion from a ≈20 wt. % masterbatch made using an internal mixer and a first dilution which was checked at 4.5 wt. %. A second series was made from the 0.5 wt. % batch in a microcompounder to reach loadings from 0.05 to 0.20 wt. %. Appendix B shows pictures and spectra of spectroscopic standards made from these batches, 5 spectra by sample and no normalization or numerical offset. Even at 0.05 wt. %, the obtained sample was totally black to the naked eye, visually difficult to differentiate from other samples. Grey material was obtained from purging the apparatus but carbon black was not detectable through TGA. Baseline shift and distortion through ATR defect steadily follows the carbon black rate. ABS characteristic peaks heights do not seem to evolve. The concentrations between 0.05 and 0.20 wt%, in light pink display very close spectra. The magnification on 2100 to 2000 cm^{-1} shows that the baseline progressive shift is still observable even though in the same order of magnitude than repeatability.

To quantify previously described phenomena, Fig. 5 shows integral values obtained from the spectra in order to quantify the observed baseline shift and intrinsic signals intensity. Fig. 5 a) shows signals chosen to evaluate these phenomena: C-H stretching from 3100 to 2800 cm^{-1}, both aliphatic and aromatic; C≡N stretching from 2255 to 2220 cm^{-1}; aromatic C-H bending from 800 to 720 cm^{-1}. Area between spectrum and a straight line drawn at the base of each peak were considered in this case. No normalization but repeatability was applied as the whole range should be impacted by effects to qualify. As no peak should be spared, none can serve as a reference for normalization. A baseline indicator was chosen by integration between spectra and the X axis on the 2100 to2000 cm^{-1} range. This choice was made because this range is free of signals attributed ABS, degraded ABS (Signoret et al., 2020) or other parasites as moisture. Also, integration averages the impact of individual values on this range, thus attenuating noise perturbation. Finally, this range was little affected by ATR deformation.

Fig. 5 b) shows that results dispersion is important on specific polymer signals and hampers a clear discussion. However, C≡N and C-H stretching signals seem to slightly decrease with also a reduction in

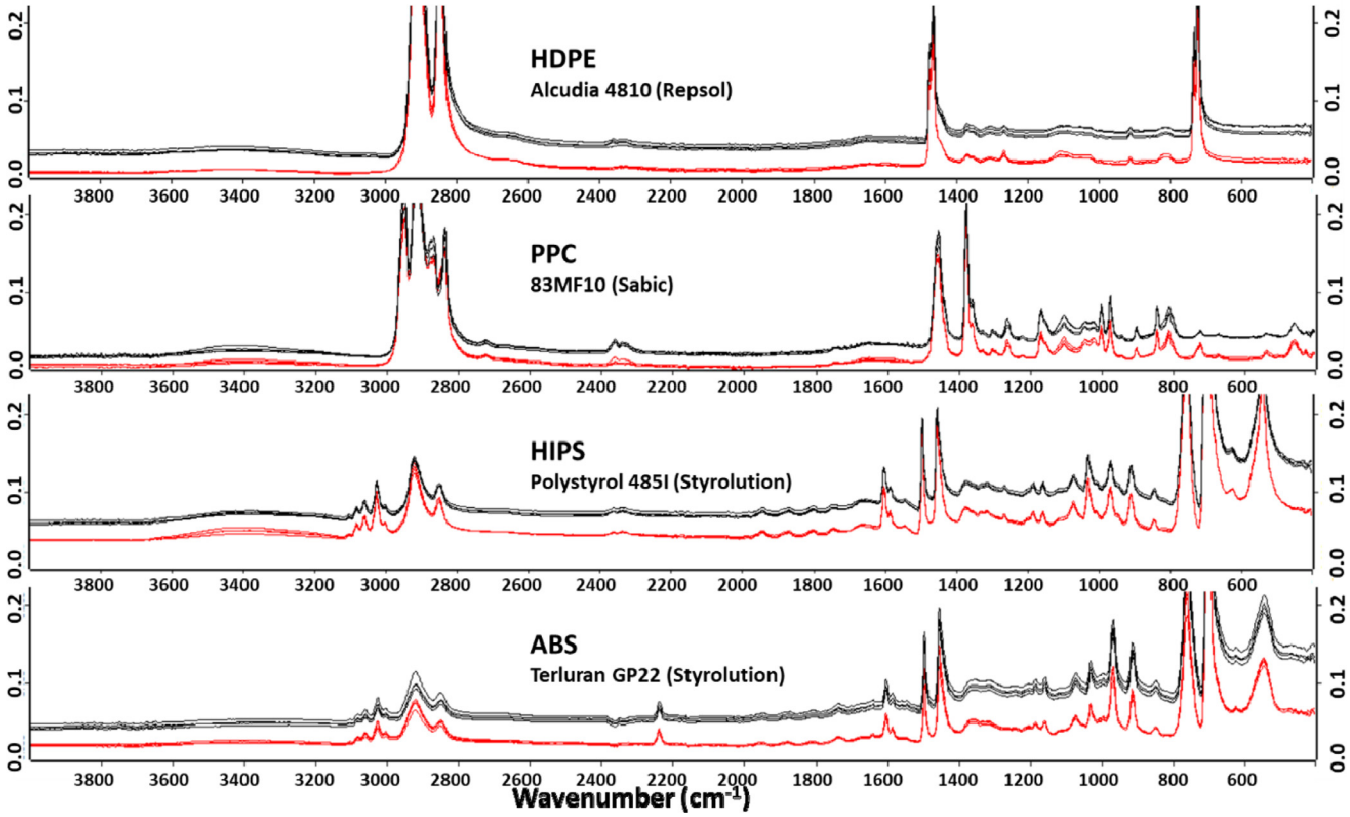

Figure 4. MIR spectra of virgin (red curves) and 2 wt. % carbon black loaded (black curves) polymer standards – PE, PP, HIPS & ABS – 4 spectra by sample, no normalization or numerical offset

dispersion. Polymer lesser absorption could be explained as it receives less incident signal because of carbon black and as its reflected signal gets also partially absorbed. Aromatic C-H does not show a decrease and could even exhibit a reduction in dispersion toward higher values. These contradictory trends can be explained by the previously observed ATR deformation, fostered by carbon black, which promotes absorption at low wavenumber. Potential effects of pi-stacking between carbon black and aromatic cycles of ABS seem unlikely as this pigment stays under an agregated form, thus not very well dispersed. It is also partly oxidized and does not exhibit a highly organized structure. Purer, better dispersed and better structured forms of mineral carbon, as nanotubes, graphite or graphine could however exhibit pi-stacking interactions.

Fig. 5 c) displays the chosen baseline indicator evolution with carbon black concentration, which proves to be rather linear on the considered scope, respecting the Beer-Lambert law. Last points at 4.5 wt. % tend to be above the regression, probably because of the ATR effect. Despite the important values dispersion, the correlation factor is rather satisfactory ($R^2 = 0.986$). The 1.98 intercept value is coherent to the values of virgin samples. Low loading samples do not seem to align perfectly as seen on the magnification. Concentrations were too low to be confirmed by TGA. As they were made differently, differences in dilutions with other samples could explain this. It should be emphasized that differences of polymer nature, chosen shape, especially surface aspect and acquisition quality strongly disturb these correlations. Here, data were well fitted because all above-mentioned parameters are almost identical even though results are pretty dispersed.

3.2.4. *Real waste samples*

Thirty-seven black colored samples among the stock were analyzed using TGA. Seven had undetectable carbon black levels (below 0.1 as other fillers were also considered here). Twenty-one had concentrations between 0.5 and 2.0 wt. %. Six others had concentrations up to 4 wt. %. Two PVC samples showed 8 and 18 wt. % which could be caused by other additives as PVC is often heavily formulated. Identification through FTIR-ATR was not challenged. Baselines and peak heights were more influenced by surface aspect and acquisition than measured carbon black concentrations. Indeed, ATR is very sensible to the contact quality between the sample and the ATR crystal, a default which does not transpose to HSI as measure is done remotely. However, other sources of acquisition degradation could be expected, as spatial non-uniformity of infrared irradiance, or sensibility to surfaces orientation and objects heights.

As an exception, one PP sample, whose spectrum is shown on Fig. 6, presented a carbon black loading rate evaluated around 25 wt. % in TGA. The first ABS masterbatch, measured at 21 ± 2 wt. %, is also plotted for comparison. However, because the high carbon black content prevented disk injection for rheological reasons, test bars were injected instead. This waste sample had the mention “Velostat” which is described as conductive polymer (Mazaheri et al., 2009). This is consistent with the high carbon black loading measured. Its spectrum baseline is strongly slanted (ATR defect), going from 0.03 to 0.08 A.U., showing a strong absorption from carbon black, whereas intrinsic signals amplitude is below 0.02 A.U. Also, the bottom of the peaks is strangely slanted. This could be explained by a deficient response of Fourier Transform to phase shift (Keeler, 2004; Ledford et al., 1980). The spectrum is however visually recognizable as PP, with four peaks for aliphatic C-H stretching from 2840 to 2950 and two peaks at 1450 and 1375 cm^{-1} respectively for C-H bending of CH_2 and CH_3. The 21 wt. % ABS reference however is hardly recognizable as its signals are generally weaker than PP on the whole MIR range through ATR (Signoret et al., 2019b). Only the strongest signals, aromatic C-H deformation at 760 and 700 cm^{-1}, are clearly visible whereas others seem only baseline defects. This hints that only the strongest signals will survive. Interestingly enough, even on such a distorted spectrum, peaks

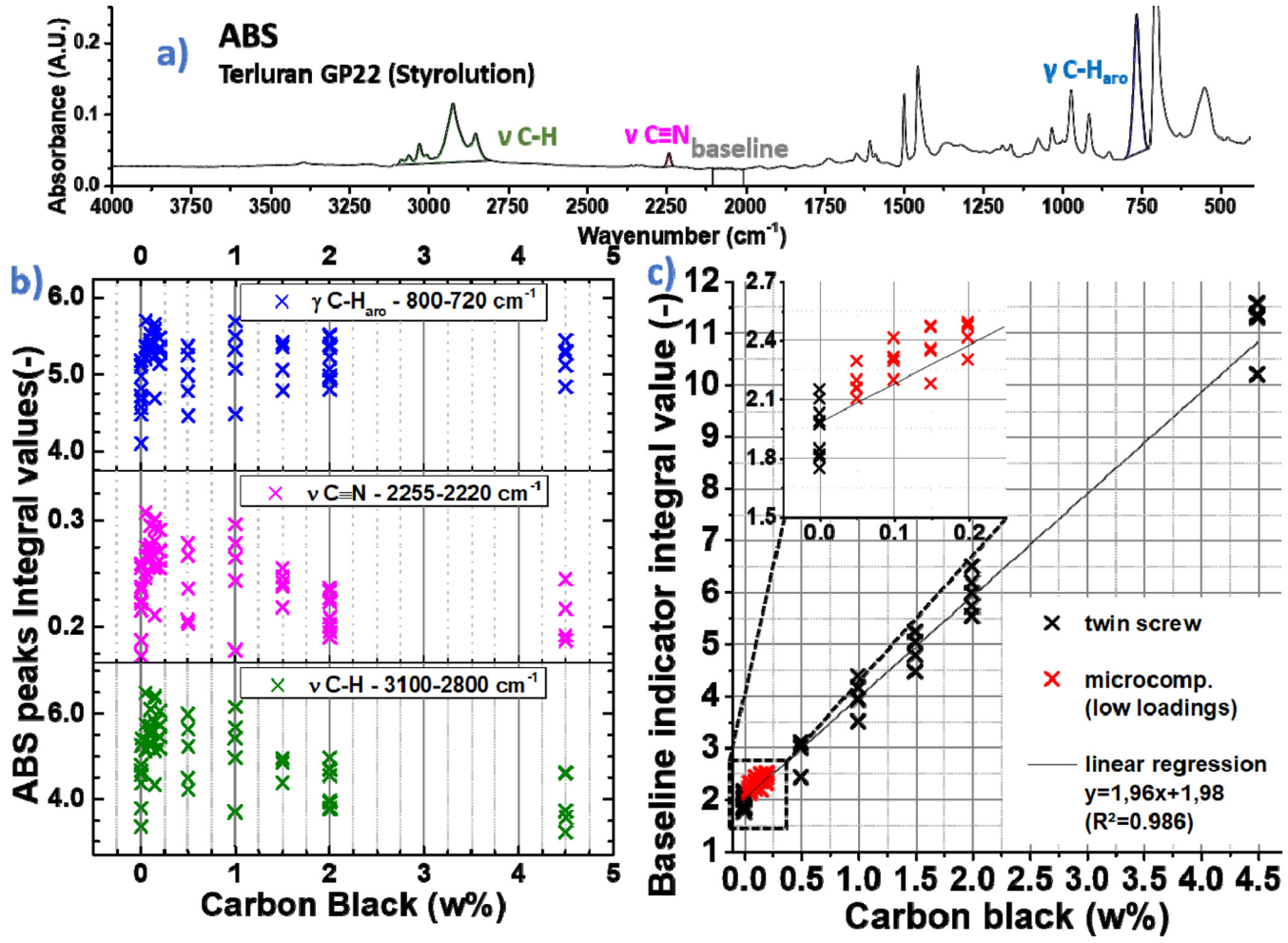

Figure 5. a) Integration zones on ABS FTIR-ATR spectra – green, pink and blue for b), grey for c); b) Intrinsic peaks integrations evolution with carbon black loading rates; c) Baseline "height" evolution with carbon black loading rates – no normalization, 5 measures/batch, 4 cm^{-1} resolution and 16 scans by acquisition

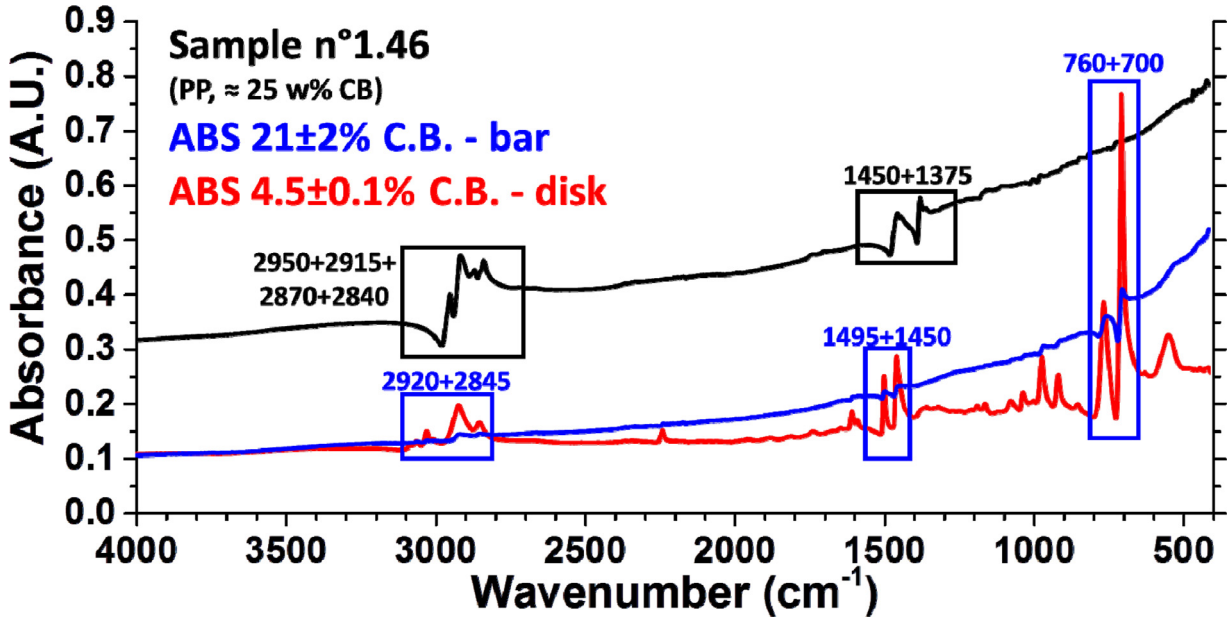

Figure 6. MIR comparison of sample n°1.46 (exception within waste stock) to ABS standards at 4.5 and ≈21 wt. % carbon black – sample identified as PP loaded with ≈25 wt. % carbon black – no normalization, baseline correction or numerical offset – black frames for PP peaks, red for ABS

retain their exact wavenumber. Finally, baselines for 4.5 and 21 wt. % overlap for the highest wavenumbers whereas the 21 wt. % spectrum should be far above, closer to the waste sample as they share close concentration. This indicates that acquisition was not optimal for the heavy loaded sample, adding to the poor visibility of characteristic signals. If signal is still sufficient in industrial conditions for such loadings, strong correction of baseline could be applied to make the spectrum exploitable despite the loss of information.

3.2.5. Conclusions on carbon black impact on MIR spectra

Because of its chemical nature, carbon black strongly absorbs from UV to NIR, even at low loadings as 0.5 wt. %, conferring its color, its protecting ability toward polymers and the current difficulty to sort most of dark plastics in an economical way. It displays a continuous absorption in MIR, but in a way less dire manner, especially for the lowest wavenumbers. For concentrations typically applied for coloration / protection purposes, between 0.5 and 2.0 wt. %, identification is not impacted for FTIR-ATR. Similar results could be expected that MIR-HSI is also whereas NIR-HSI is generally reported ineffective (Beigbeder et al., 2013; Huth-Fehre et al., 1995; Serranti et al., 2012).

The main noticed effect of carbon black in FTIR-ATR is a shift of the baseline toward higher absorbance, proportional to concentration, according to the Beer-Lambert law. The ATR distortion of baseline is also promoted. Higher loadings (> 20 wt. %) corresponding to very specific conductive applications in thermoplastics and mechanical reinforcement in elastomers are disruptive toward identification which is still possible depending on the material. However, as infusible materials, elastomers should be industrially segregated as unsuitable to mechanical recycling. Thus, highly distorted spectra, which hint for high carbon black concentration, should lead to refusal.

3.3. Usual mineral fillers

3.3.1. Powder references

Calcite and talc are widely used as fillers, to reduce costs mainly for the former, but they also bring stiffness for the latter and unfortunately density for both (Maris et al., 2015). Titanium oxide (TiO_2) is widely used as an opacifier and a whitening agent. With kaolin, these three additives were analyzed in FTIR-ATR, directly in powder form (Fig. 7). They display very few and very weak signals in the MWIR range, even none for TiO_2, leaving their lines almost empty in the corresponding chart in *supporting information*. However, corresponding wavenumbers are in usually empty ranges: three sharp signals between 3620 and 3695 cm^{-1} for kaolin; a bump at 2510 cm^{-1} for calcite; three signals at 3675, 3555 and 3415 cm^{-1} for talc. In the LWIR range, they display very strong, very large (except for kaolin) and distinctive signals: for kaolin a very characteristic quadruplet 1114, 1032, 1008 and 914 cm^{-1}, and three signals between 430 and 540 cm^{-1} (off range); for calcite a very broad asymmetric signal at 1406 cm^{-1} and a very specific signal at 874 cm^{-1}; for talc a very broad signal at 1010 cm^{-1}, a very specific signal at 670 cm^{-1} and three intense signals between 465 and 425 cm^{-1} (off range); for TiO_2 a wide and strong signal from 800 to 500 cm^{-1}, at the limit of LWIR. It is interesting to note that the 670 cm^{-1} signal for talc and the 873 cm^{-1} for calcite are in rather empty columns within the LWIR chart (*supporting information*), thus enabling rapid identification. However, confirmation should be done with the large and intense signals.

3.3.2. Real waste samples

Because of the specificity of these wavenumbers (totally or almost alone in their columns of the charts in *supporting information*), even weak signals could be easily seen on numerous plastic waste samples, every encountered PVC and most of polyolefins samples. On the displayed example of polymer waste in Fig. 8.a) and b), both calcite and talc can be very clearly seen in LWIR, especially with the specificity of respectively the 873 and the 670 cm^{-1} peaks, which enabled rapid identification for most of the waste stock. Impressively enough, the fillers very weak peaks in MWIR are also visible on part a). The 37 dark plastic waste samples analyzed above in TGA for their carbon black concentrations were also studied in SEM/EDX for other additives. Most of the polyolefins contained talc and/or calcite and spectroscopic marks described here were observed each time. Residual weights in TGA

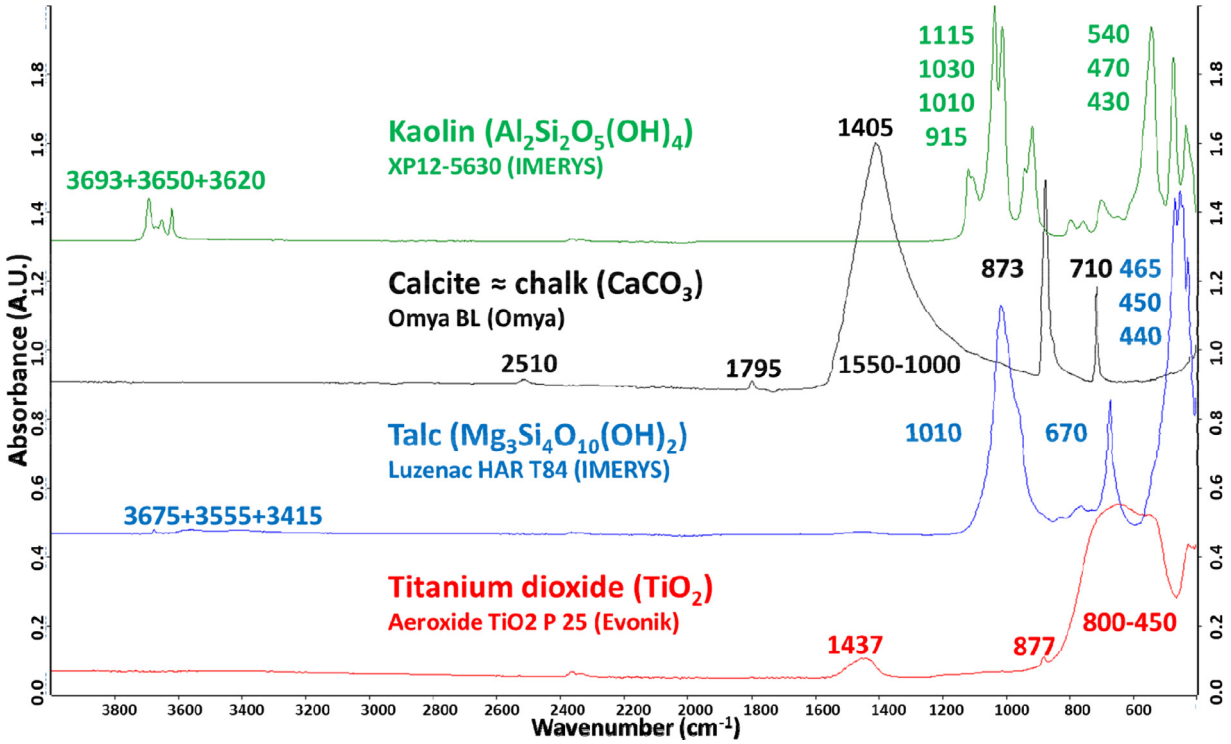

Figure 7. MIR spectra of common mineral fillers – kaolin (green), calcite (black), talc (blue), titanium oxide (red) – wavenumbers in corresponding colors

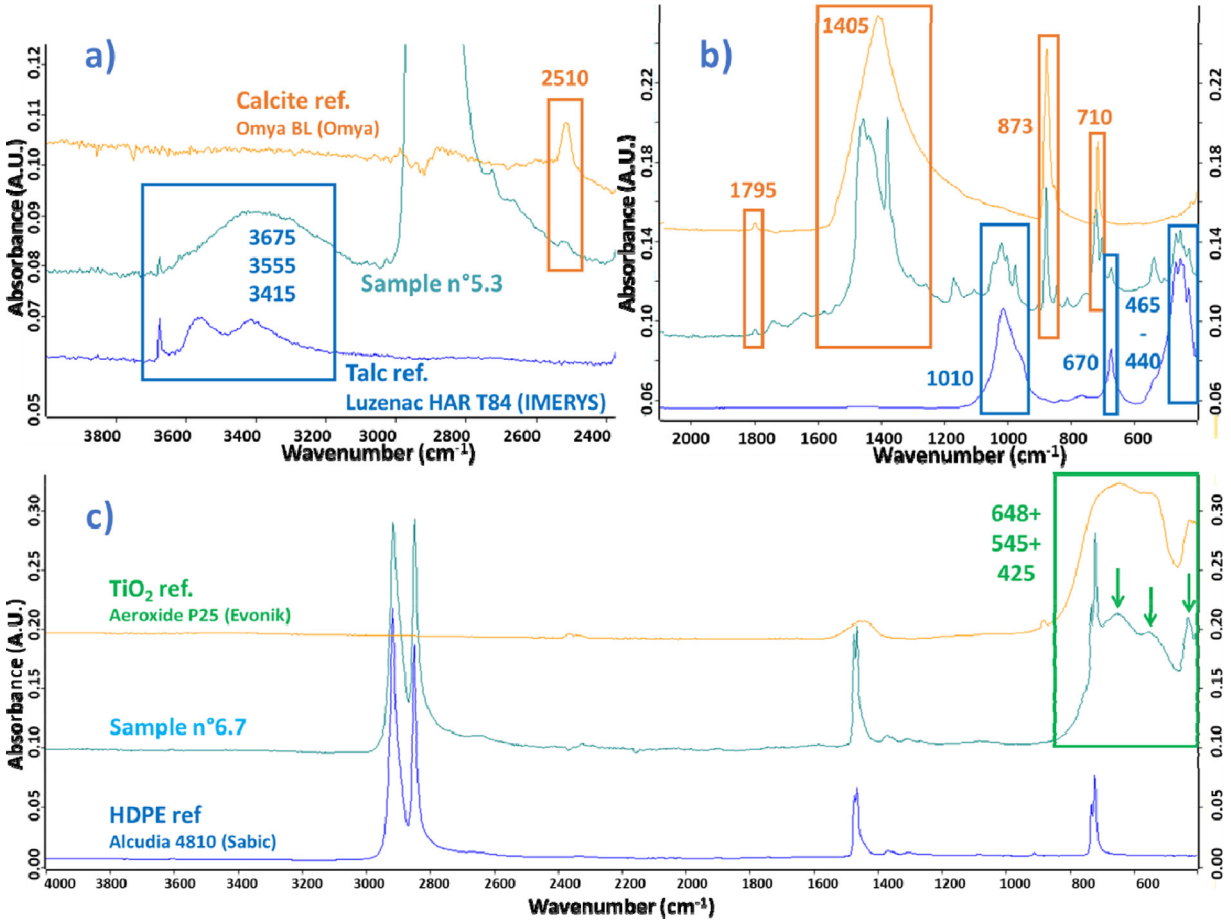

Figure 8. MIR spectra of a waste samples containing spectrally visible fillers – a) & b) A sample with both talc (blue frames) and calcite (orange frames) visible, from 4000 to 2400 and from 2100 to 400 cm^{-1} – c) A sample with visible titanium dioxide (green frame)

indicates that typical loading rates were between 10 and 20 wt.% which is coherent with industrial use. Only 3 styrenics were found to contain fillers according to EDX and characteristic peaks were visible on the spectrum of only one of them.

The signal from 800 to 450 cm^{-1} of TiO_2 was indicated in orange in the charts because it was less visible within real samples as its loading rates were probably weaker as it is a pigment rather than a filler. Indeed, spectral marks of TiO_2 were formally confirmed on only one sample (Fig. 8.c)), particularly white, of the hundred available ones even if SEM-EDX revealed traces in 6 of the 37 analyzed samples. Its main signature is confined between 500 and 600 cm^{-1} and is represented by a round band. The other weak round peak at roughly 1440 cm^{-1} overlaps with CH_2 deformation and is thus masked in numerous polymers (as polyolefins, styrenics or polyamides). Use of other additives, especially talc, and bad acquisition leading to strong ATR baseline defect often lead to doubts about signals which could indicate TiO_2 presence. In HSI application, almost no signals are specific, except for a rise on the lowest wavenumbers in LWIR. No sample was found with kaolin peaks, in accordance with the current limited commercial use of this filler. If present in sufficient amount, it could be detected through its peaks between 3693 and 3620 cm^{-1} since peaks of talc between 3675 and 3415 cm^{-1} were visible despite their low intensity. Also, its specific peaks at 1115 and 540 cm^{-1} should enable identification, even in presence of talc or calcite that could overlay its signals.

3.3.3. Conclusions on usual mineral fillers

In general, talc and calcite were the main additives to display visible marks on the real waste samples spectra among the studied stock. It can be assumed that other additives are in too low concentration or do not exhibit important enough infrared signature. Interestingly enough, after sink-float separation, most floating polyolefins still displayed peaks characteristic of a filler, even if weaker than in sinking ones. Combined with TGA or calcination, FTIR-ATR can rapidly give natures and concentrations of fillers, instead of more laborious methods as ICP or X-rays fluorescence. Described fillers can be seen in MWIR even though their specific signals are very weak and diminished acquisition parameters will surely make them undetectable. Consequently, polymer identification should not be disrupted in MWIR. It is not the case in LWIR because of their large signals, which can partially mask specific signals of polymers. It is thus important to identify and take into account their patterns when building classification algorithms. By considering these signals as those of fillers, it could then facilitate the matrix identification. Filler detection could also be a segregation tool, as it would be devoted mainly to polyolefins and PVC. Finally, it could be interesting to check additives effects on NIR. If impacts are important on identification, it could render MIR more interesting, even in the case of light-colored plastic waste. However, a real comparison of the two technologies in such waste stocks should be pertinent at least at pilot scale.

3.4. Flame retardants

3.4.1. Powder and polymer references

Flame retarded polymers are widely used in electronic and electrical equipment and furniture as they can be subjected to fire hazards. However, many flame retardants (FRs) which were popular a few decades ago because of their performance at low loadings are now progressively forbidden, or at least greatly depreciated in reason of their health and environmental hazards, especially halogenated FRs

(Aldrian et al., 2015; Peeters et al., 2014; Schlummer et al., 2005; Stenvall et al., 2013). It is thus interesting to detect these now forbidden or phased out FRs within waste plastics. Elemental techniques as X-ray transmission or fluorescence, or LIBS, are rather performant. However, mainly X-ray transmission is nowadays applied in industrial and economic conditions. Unfortunately, this technology is limited towards distinction between elements heavier than oxygen within polymeric matrices.

Because of their efficiency at low loadings, brominated flame retardants were quite popular and can be found from a few percent to about 15 wt. % within plastic waste (Guzzonato et al., 2016b; Schlummer et al., 2005). Tetrabromobisphenol A (TBBPA) and Hexabromocyclododecane (HBCD) are amongst its main representatives (Puype et al., 2019). Antimony trioxide (Sb_2O_3) is also often used in synergy with these FRs. As only TBBPA was available in sufficient quantities to product plastic samples, HBCD and Sb_2O_3 were only studied as powders. Less frequent, chlorine based FRs as dechlorane are also found (Schlummer et al., 2005). Because of the ban of some halogenated FR, phosphor based FRs as ammonium polyphosphate (APP) are getting more and more popular (Peeters et al., 2014). FRs specifically cited above were chosen to produce standard samples because of their common use within plastics and because they were rapidly available for experiments.

As seen on Fig. 9.a), ammonium polyphosphate (APP) displays a very wide signal from 2700 to 3300 cm^{-1}. It covers almost all the MWIR range as seen in the associated chart in *supporting information*. Three mounts culminate at 2885, 3015 and 3165 cm^{-1}, associated to the O-H bounds of the phosphate groups. The one associated to the highest wavenumber is particularly visible on formulated samples. For styrenics, this large band tends to mask polymer characteristic signals, potentially challenging identification. APP displays numerous, rather strong signals and broad signals (50 to 100 cm^{-1} wide) in the LWIR area. The 1246 cm^{-1} stands out but the 4 peaks from 1080 to 798 cm^{-1} offer a very distinctive pattern. The three peaks below 550 cm^{-1}, thus out of the LWIR range, are reminiscent of talc but at higher wavelength and more spaced out. The 1425 cm^{-1} peak, above LWIR, tends to add up to the very common 1450 to 1470 cm^{-1} peak associated to CH_2 deformation. The 1680 cm^{-1} is too weak and present in an area often disturbed by carbonyl species produced by ageing. Overall, by its numerous and large signals, APP can complicate identification as it becomes the main component of the spectrum in the MWIR and LWIR ranges. Interestingly enough, the 1375 cm^{-1} and 760 to 750 + 700 to 695 cm^{-1} peaks, respectively characteristic of PP and styrenics fill the gaps between APP peaks. It would be also the case with the 730 to 720 cm^{-1} signal of PE. In the range between MWIR and LWIR, roughly from 2000 to 1400 cm^{-1}, APP does not disturb identification, which is mainly based on the carbonyl peak (Signoret et al., 2020) (as PC, PMMA, PET and PA).

Dechlorane C25+ (Fig. 9.b)), a chlorinated FR, displays rather weak C-H stretching signals at 2950, 2910 and 2850 cm^{-1}, typical of aliphatic C-H stretching, in accordance to its chemical nature. These wavenumbers are already covered by most polymers. This additive seems thus practically impossible to detect in MWIR. However, in LWIR, it possesses very numerous, strong and sharp signals. The 1282 cm^{-1} is characteristic as it is in an empty column in the LWIR chart. The several peaks, from 1168 to 831 cm^{-1}, covers a more occupied area as none of them are in empty column and they tend to make the obtained pattern way more complex. The six peaks from 763 to 592 cm^{-1} possibly correspond to C-Cl stretching as there are 12 chlorine atoms within the structure which can vibrate with multiple symmetrical and asymmetrical modes. With almost equal heights of four of them and equal wavenumbers gaps between the first three, they create a very distinctive pattern. Also, they modify the general look of the characteristic aromatic C-H deformation of styrenics, two peaks from 760 to 750 cm^{-1} and from 700 to695 cm^{-1}. Especially, a new sharp peak appears just between them. As APP, Dechlorane should be easily detected in LWIR but could disrupt the matrix identification as it complicates the spectrum. It is however probably undetectable in MWIR.

In MWIR, TBBPA is rather subtle and was mainly seen for rather high loading (34 wt. %) through its 3475 cm^{-1} peak (Liu et al., 2016), as seen squared in blue on the left part of Fig. 9.c). As well, its numerous LWIR signals are hardly visible below 17 wt. %. The 1173 cm^{-1} is probably the most visible marker. For ABS and ABS-PC, the 730 cm^{-1} is also pretty remarkable as it inserts itself just between the two aromatic C-H peaks. However, it is not visible in HIPS as the higher peak is lower (750 instead of 760 cm^{-1}) and larger, covering it. Outside of ranges covered by MWIR and LWIR, the peak at 1471 cm^{-1} is also very visible in styrenics as it inserts between the ones at 1493 and 1452 cm^{-1}. Just above, a small but sharp peak can be seen at 1555 cm^{-1} only for highest loadings. Finally, a large band at 1739 cm^{-1} is visible for higher loading but could be mistaken for polymer ageing carbonyls.

Spectra of flame retardants above, with the addition of HBCD and Sb_2O_3 are given in *appendix C* for better readability.

3.4.2. Real waste samples

Very few samples within the studied waste stock presented remarkable spectroscopic patterns of flame retardants. Accordingly, only one of the thirty-seven samples studied in SEM/EDX showed presence of flame retardant, a brominated one in this case. Except with PVC, most of marked foreign signals were associated to calcite, talc and/or ageing. PVC often displays a peak at 1730 cm^{-1} associated to phthalate plasticizer and/or stearate thermal stabilizers (Signoret et al., 2019b). This can be explained as the waste stock was not primarily chosen to study flame retardants and probably went through X-ray sorting. Fig. 10 shows two waste samples which were identified as containing flame retardants. The n°5.11 was identified as HIPS and several Dechlorane peaks were observed, especially at 1470, 1282, 592 cm^{-1} and between 1168 and 831 cm^{-1}. The peak at 763 cm^{-1} is hinted through a subtle shoulder of the 750 cm^{-1} peak of HIPS. Sample n°5.30 was identified as TBBPA loaded ABS, with especially the double peaks of 1272 + 1238 cm^{-1}, the one at 1555 and the one at 867 cm^{-1}. The 730 cm^{-1} peak is also well visible between the styrene peaks and the 1471 cm^{-1} is seen as a shoulder. Fig. 10 highlights that both Dechlorane and TBBPA creates “interstitial” peaks within styrenics, between the 1452 and 1493 cm^{-1} peaks (outside of LWIR) and between 750 + 695 (PS) / 760 + 700 (SAN) (at the limit of LWIR). However, they are not very intense and pretty close from other peaks. Depreciated resolution and sensibility can be fatal to their detection.

3.4.3. Conclusions on flame retardants

It appears that Dechlorane and APP are well visible in LWIR (from 8 wt. % and 16 wt. % loadings respectively), especially with significant and numerous signals (Dechlorane) or broader signals (APP). TBBPA is harder to identify unless a high loading (34 wt. % here) is applied. APP also strongly distorts MWIR spectra with a large baseline elevation from 2600 to 3400 cm^{-1}, which could be mistaken with acids but a bump at 3165 cm^{-1} is specific. Dechlorane is impossible to detect in MWIR and TBBPA O-H stretching can be spotted at 3475 cm^{-1}, but only for higher loadings.

Flame retardants industrial detection in MIR seems difficult as signals are subtle, except for APP which could disrupt polymer recognition as its bands could mask the characteristic polymer spectra. Further studies on a larger scope of flame retardants (especially PBDE, polybromodiphenylethers) and a waste stock rich in flame retarded plastics could ensure their detection and pseudo-quantification in FTIR without relying on heavier techniques as XRF. Hyperspectral detection seems compromised and industrial segregation of halogenated plastics should be done thanks to a more reliable technology as industrial XRT or XRF. However, this also means that polymer identification in MIR-HSI is unlikely to be hindered by flame retardants presence.

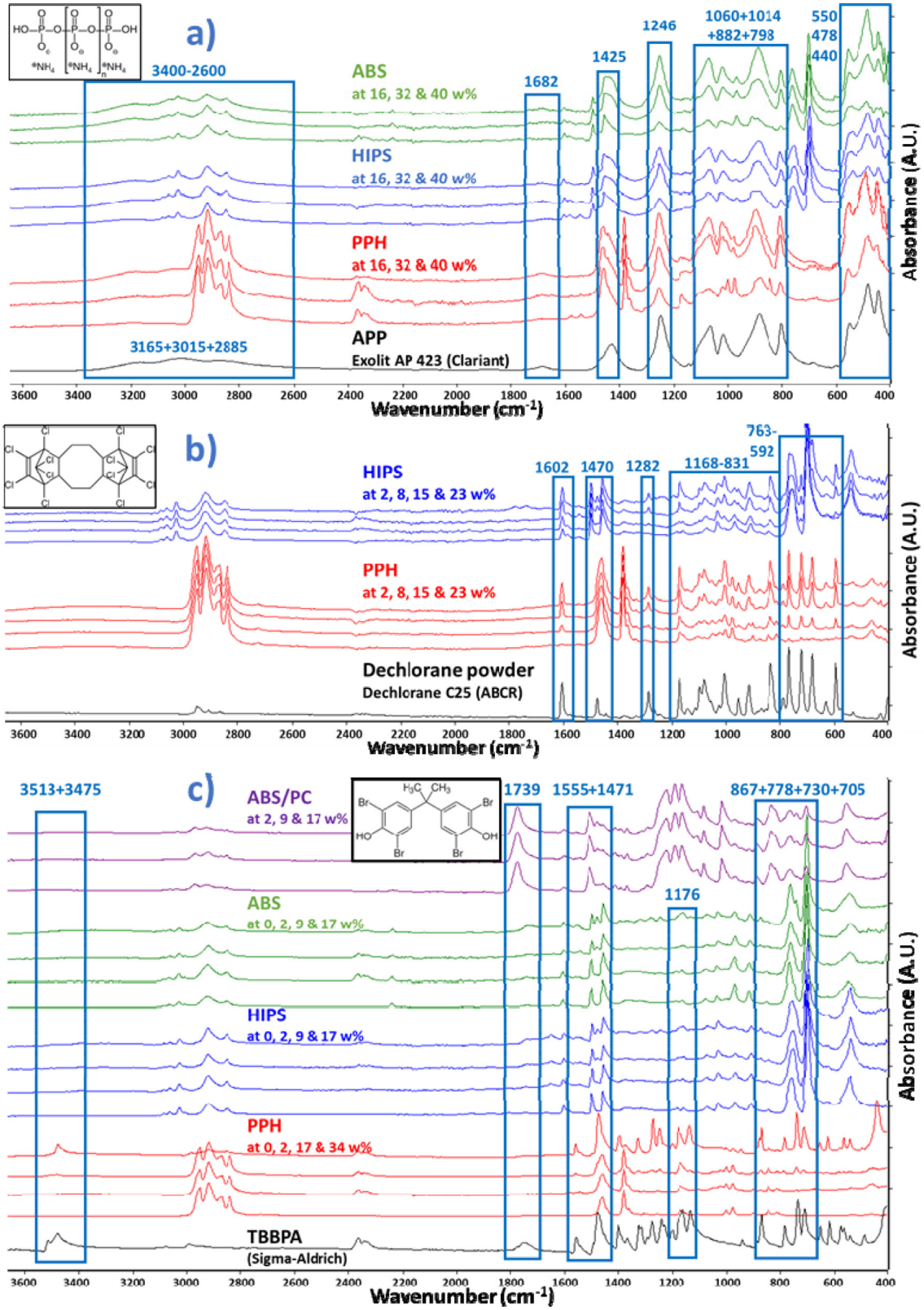

Figure 9. FTIR-ATR spectra of different standards formulated with APP (a), dechlorane (b) or TBBPA (c) – blue frame for FR characteristic peaks seen within polymer references

3.5. Complex samples examples

Several "complex" samples were found among the plastic waste stock, in the sense that they correspond to several materials bonded together and could negatively affect sorting operations. Fig. 11.a) shows a few examples. The top one (n°1.9) corresponds to an ABS square, characterized by the acrylonitrile peak at 2237 cm^{-1} framed in green, in which was included an elastomeric cylinder. This part's

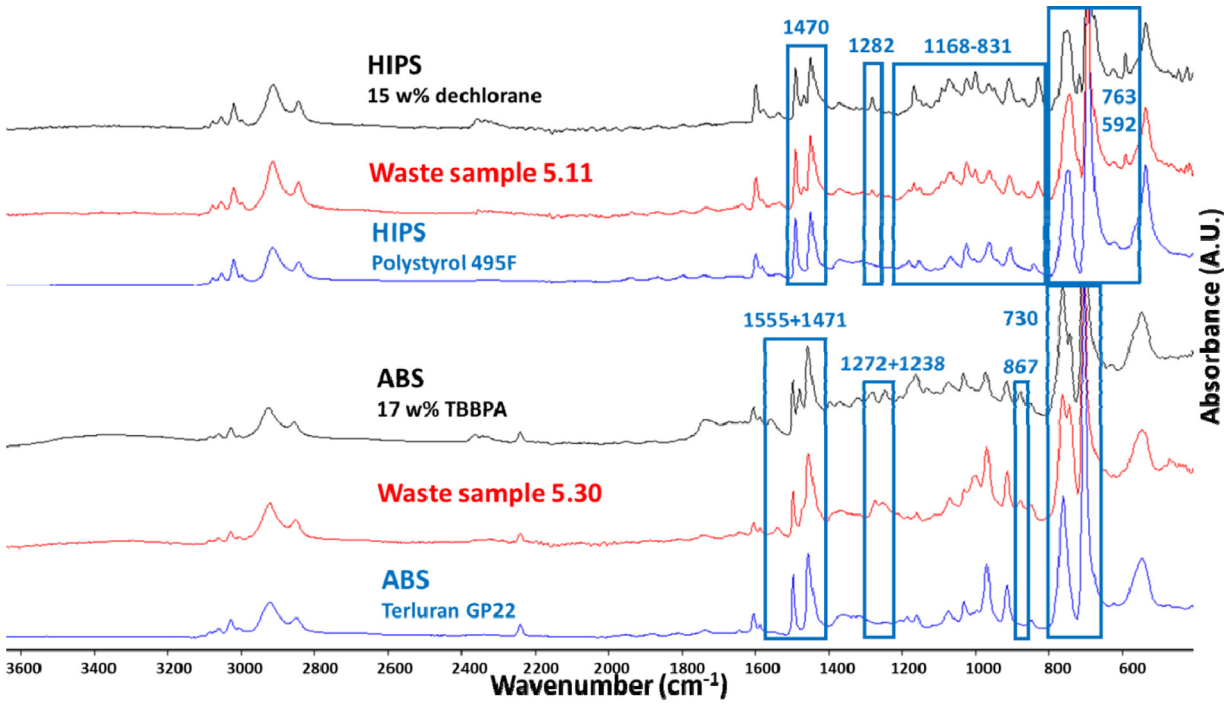

Figure 10. Spectra comparison of two waste samples respectively with virgin and 15 wt. % Dechlorane HIPS references and with virgin and 17 wt. % TBBPA ABS references– blue frame for RF characteristic peaks seen within polymer samples

spectrum is heavily distorted. Its initial baseline (shifted here for readability) varies between 0.5 and 0.6 A.U. of absorbance for about 0.1 to 0.2 U.A. for intrinsic peak heights. Peaks also display defaults at their base, reminiscent of the ≈20 wt% carbon black loaded PP and ABS of Fig. 6. High carbon black loading is coherent with the elastomeric nature of this component. Identification is here challenged, especially as this study focused on thermoplastics. The two peaks between 2920 and 2850 cm^{-1} could hint for an important ethylene base. Peaks roughly at 1000 and 800 cm^{-1} could correspond to vinylic C-H deformation but do not match to PB (910 and 965 cm^{-1}). Polyisoprene is a possible candidate.

The second sample (n°2.8) consists of a green bulk tinted polyethylene, identified by its simple spectrum, coated with a PVC sheet, white on one side, lighter green on the other side as seen on the picture. PVC is identified thanks to the 610 and 700 cm^{-1} peaks. A plasticizer and/or thermal additive presence is shown through the 1730 cm^{-1} peak. The last sample, n°4.19 results of the welding of two transparent sheets which could be identified as PC and PMMA thanks to carbonyl peak, respectively 1770 and 1720 cm^{-1} and characteristic C-O stretching patterns between 1300 and 1000 cm^{-1}. Interestingly enough, in the welding zone, an intermediate spectrum can be obtained, with the peaks of both polymers, especially highlighted for the dual carbonyl peaks.

Several samples were categorized as “shiny grey HIPS”. As shown on Fig. 11.b), they consist of dark grey bulk tinted HIPS with a shiny grey coating. Bulk is easily recognized as HIPS thanks to aromatic C-H bending at 695 and 750 cm^{-1} (whereas it is 700 and 760 cm^{-1} for ABS) (Signoret et al., 2019a). The shiny coating is rather thin and its spectrum, even though distorted, is heavily reminiscent of PMMA, an acrylic polymer, notably with a C=O stretching at 1724 cm^{-1}, rather specific pattern from 1480 to 1385 cm^{-1} for C-H bending, culminating peak at 1143 cm^{-1} for C-O stretching and a peak at 750 cm^{-1} for C-H rocking (Szilasi et al., 2011). Acrylic paint is thus strongly suspected, as its main monomer is also methyl methacrylate.

If analyzed on “bulk” face, these samples would be identified as HIPS. On the other side, ATR spectra are heavily distorted and cannot be confused with PMMA. Similar effects can be expected but must be checked in MIR-HSI. It can be anticipated that this supposed paint would impact also other identification technologies, as Raman spectroscopy or froth flotation. Even if not found within the studied stock, metallized ABS is rather common, especially in ELV (End-of-Life Vehicles). These objects can be expected to be hard to identify as ABS. As the metal layer will surely be problematic during mechanical recycling, it can be positive to remain unidentified.

Other common “complex” objects were also found, as electrical cables, often combining mainly copper and PVC, screwed plastic parts, elastomer pads embedded in plastic, paper or plastic label. Metallic parts were found despite magnetic sorting probably because of their rather low concentration within plastic. All these objects could negatively impact recycling. First, they can disturb identification. Secondly, they bring contaminants that can affect processability and use properties.

4. Conclusions

Nowadays, the industrial sorting of dark-colored End-of-Life plastics is an obstacle to their recycling, as one of the most spread sorting technologies, Near-Infrared Hyperspectral Imagery (NIR-HSI) is unable to perform this task. Mid-Infrared HSI (MIR-HSI) is one the potential answers to this issue.. Consequently, its laboratory equivalent, Fourier-Transform Infrared spectroscopy (FTIR), was here studied to evaluate the theoretical limits of its industrial equivalent. Possible dangers of decreased acquisition parameters were shown in the first part of this study. Resolution depreciation leads to convolution of close signals and acquisition time decrease alters Signal-to-Noise ratio (SNR). This is particularly detrimental to small and close peaks. Atmospheric species, namely carbon dioxide and water are visible in both MWIR (5000 to 2000 cm^{-1} or 2 to 5 μm) and LWIR (1350 to 700 cm^{-1} at max or 7.4 to 14.0 μm) but should not disturb polymer identification as covered ranges or signal natures are different.

Carbon black, which is prohibitive for polymer sorting in NIR-HSI, also impacts MIR spectroscopy. The main feature is an elevation of baseline. Identification should however still be possible, especially with relatively low loadings associated to coloration and UV-protection (0.5

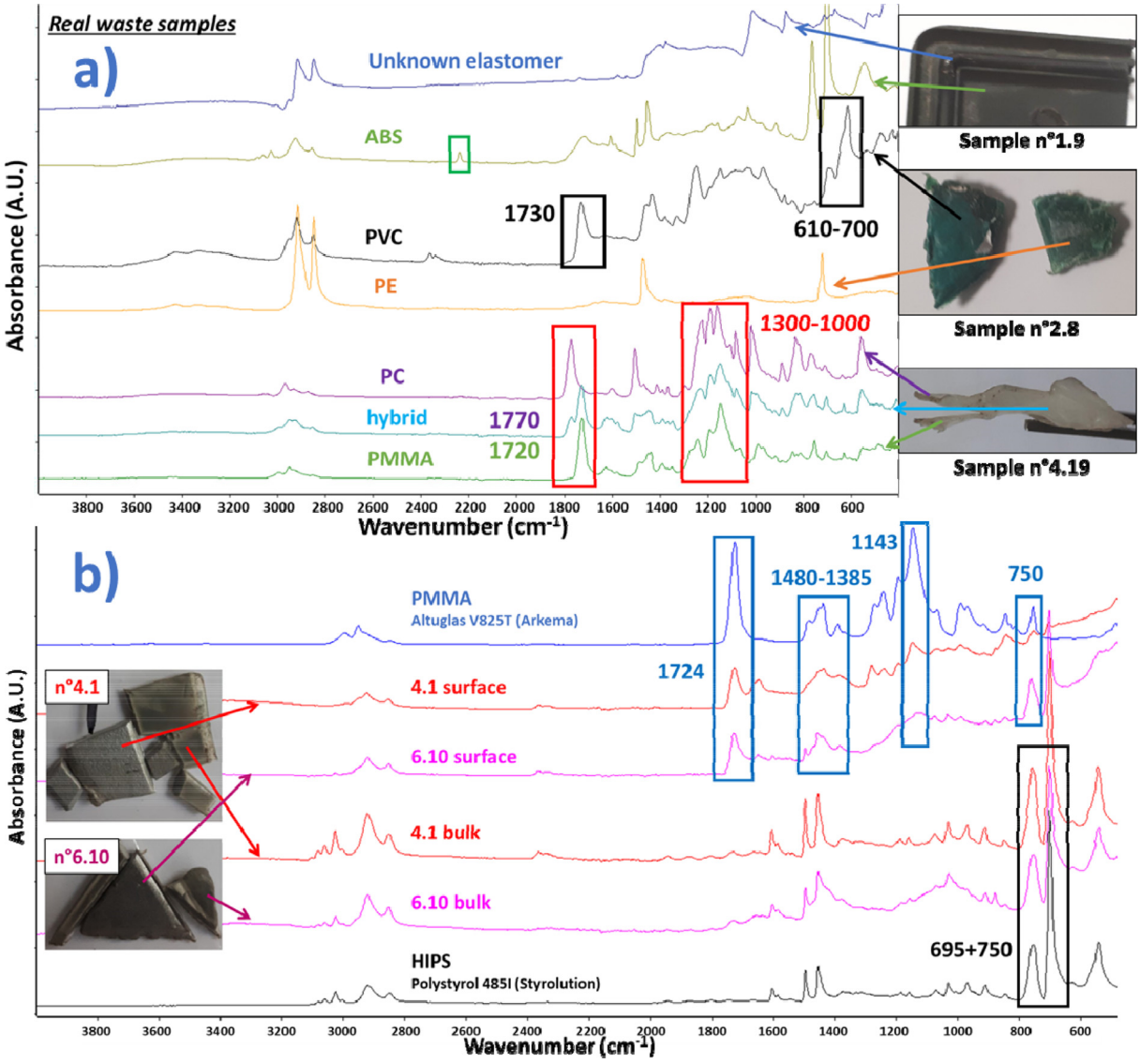

Figure 11. Examples of complex real waste samples – a) several polymers within a sample - b) painted HIPS, spectra of both faces and comparison to PMMA and HIPS reference samples – blue frames for PMMA peaks, black for HIPS

to 2.0 wt. %). Higher loadings used for electrical conductivity or mechanical reinforcement (mainly elastomers) strongly distort spectra and could negatively interfere with classification algorithms.

Fillers, namely calcite, talc, kaolin and titanium dioxide, and flame retardants, namely APP, Dechlorane and TBBPA, were also described in MIR. Most of them display very few signals or none in MWIR. These signals are also often weak. Thus, they cannot be detected and will not disrupt polymer identification in MWIR. Their signatures in LWIR are generally more intense and they cover large ranges, either by very broad signals or by very numerous peaks. Then, they can severely disrupt polymer identification in LWIR. This disruption can be seen in several ways: polymer peaks are masked; additive peaks are recognized as belonging to another polymer; data amount and general signal appearance are detrimental to algorithmic treatments. In this way, it is important to incorporate these pieces of information or, even better, altered spectra in a working database. In this purpose, these signals were here collected and described in this study.

Additives studied here were conditioned by what was rapidly available and what was identified within the studied plastic waste stock, mainly calcite and talc. Numerous other additives, especially flame retardants or stabilizers, are to be found within plastic waste. Thus, an exhaustive referencing in FTIR-ATR could be really interesting for both fast but rich laboratory analysis and possible impacts on industrial sorting. After these signals are qualitatively identified, they could explain significant differences found in a statistical study, especially with the use of classification algorithms. To consolidate these results, it would be then necessary, with the help of automatized methods, to extend the study to a larger waste stock, especially richer in flame retarded samples.

Funding

This work was supported by BPI France via the FUI 20 (Fonds unique interministériel) grant.

CRediT author statement

Charles Signoret (PhD student): Writing - original draft, Conceptualization, Methodology, Investigation and rewriting revision manuscript.

All the authors: Visualization, Investigation and validation.

Didier Perrin & Patrick Ienny: Supervision

Didier Perrin: Editing, Data curation, Reviewing.

Declaration of Competing Interest

The authors declare that they have no known competing financial interests or personal relationships that could have appeared to influence the work reported in this paper.

Acknowledgements

The authors would like to express their appreciation toward Benjamin Gallard, Robert Lorquet, Loïc Dumazert and Jean-Claude Roux from C2MA for technical support, respectively for polymer processing, spectroscopy experiments, thermal characterization and SEM/EDX analysis. Marc-Adrien Tronche, PhD student at ENSCM, is also thanked for his advice about carbon black managing. Suez and Pellenc ST are gratefully acknowledged for partnership in this work. Finally, the authors are very thankful to Allize-Plasturgie for providing the numerous references of the Matériautech used in this work.

Appendix A. Examples TGA curves for concentration control of carbon black loaded ABS standard samples – under nitrogen until 670°C, oxygen beyond - magnification on gas switch zone

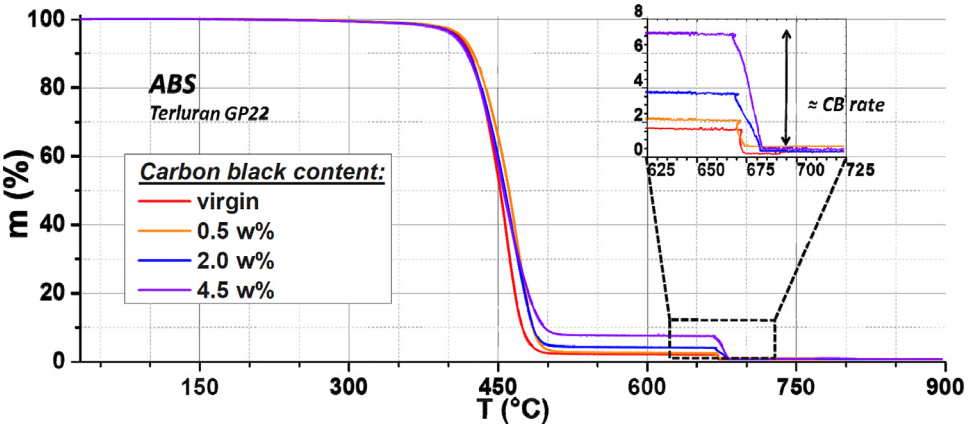

Appendix B. MIR spectra of ABS at different carbon black loadings between 0.05 up to 4.5 w% - 5 spectra by sample, no normalization or numerical offset – magnification on 2100-2000 cm-1 for low loadings – pictures of corresponding samples

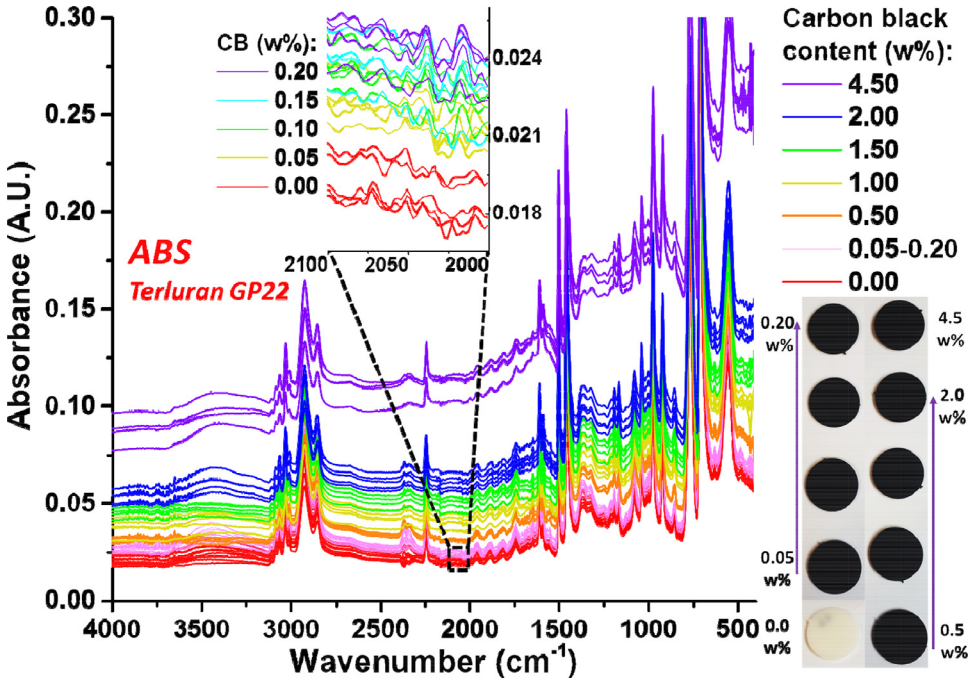

Appendix C. FTIR-ATR (MIR) spectra of flame retardant powder references

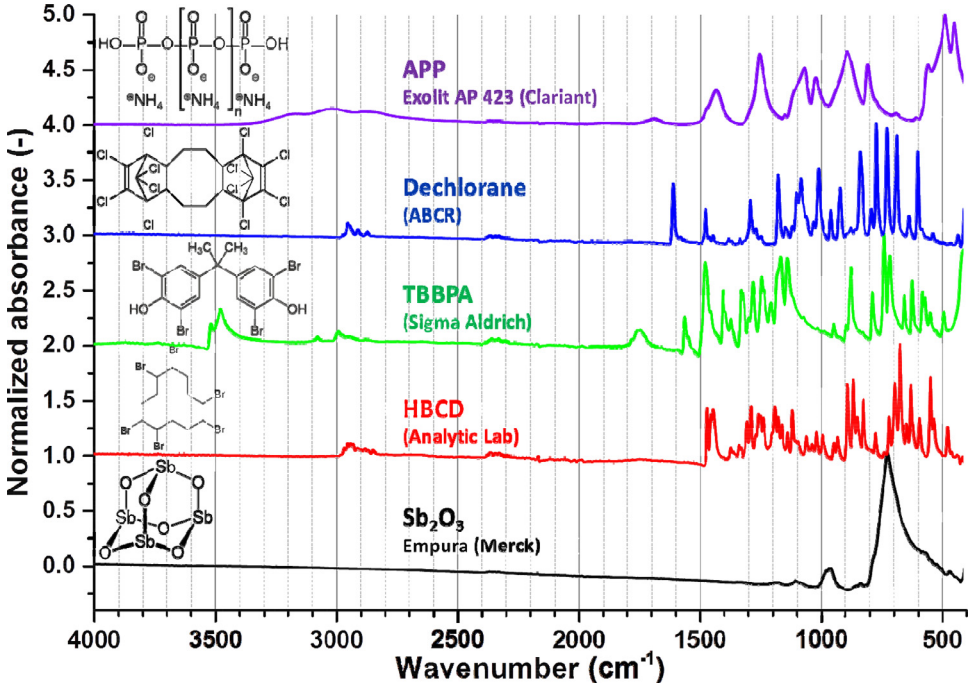

*Absorbance values normalized on max intensity

Appendix D. MWIR chart: Signals of polyolefins, PVC, POM, styrenics, additives and atmospheric species in the 5000-2000 cm^{-1} range

Families		*Species*	> 3300	*3080*	*3070*	*3060*	*3040*	*3025*	*3000*	*2995*	*2980*	*2965*	*2955*	*2930*	*2920*	*2900*	*2870*	*2860*	*2850*	*2840*	*2795*	*2735*	*2720*	*2510*	*2370*	*2340*	*2240*
Polyolefins	PE based	PEX													2914				2847								
		EVA													2916				2848								
		LD&HDPE													2915				2847								
		EPDM											≈2955		2917				2849				2725				
	PP based	PPH											2950		2916		2867			2837			2723				
		PPC											2950		2917		2868		2848	2837			2723				
Other polymers		PVC										2964			2912				2850								
		POM									2979				2921				2854		2792						
Styrenics	PS based	GPPS		3081		3059		3025	3002						2920				2849								
		HIPS		3081		3059		3025	3002						2920				2849								
		HIPS/PPE		3081		3059		3025	3002						2920				2849			2735					
	SAN based	SAN		3083		3061		3026	3003						2923				2854								2237
		ABS		3083		3061		3026	3003						2921				2851								2237
		ASA		3085		3060		3027	3003				2957	2929			2874										2237
		ABS/PMMA				3063		3026		2990			2950		2922				2847								2237
		ABS/PC				3060		3027				2967		2926			2872		2852								2237
C=O containing		PMMA								2993			2950		2922				2848								
		PC				3058	3040					2967		2932			2871										
Fillers		Talcum	3675																								
		Kaolin	3695-3620																								
		$CaCO_3$																						2509			
		TiO_2																									
Flame retardants		APP	3165					3015		2885																	
		Dechlorane											2950			2907			2850								
		HBCD										2964	2949	2928		2908	2876			2842							
		Sb_2O_3																									
		TBBPA	3515 + 3475		3074					2989		2972	2947														
Others		CO_2																							≈ 2370	≈ 2340	
		H_2O	noise > 3500																								

Appendix **E. LWIR chart: Signals of polyolefins, PVC, POM, styrenics, additives and atmospheric species in the 1400-610 cm^{-1} range**

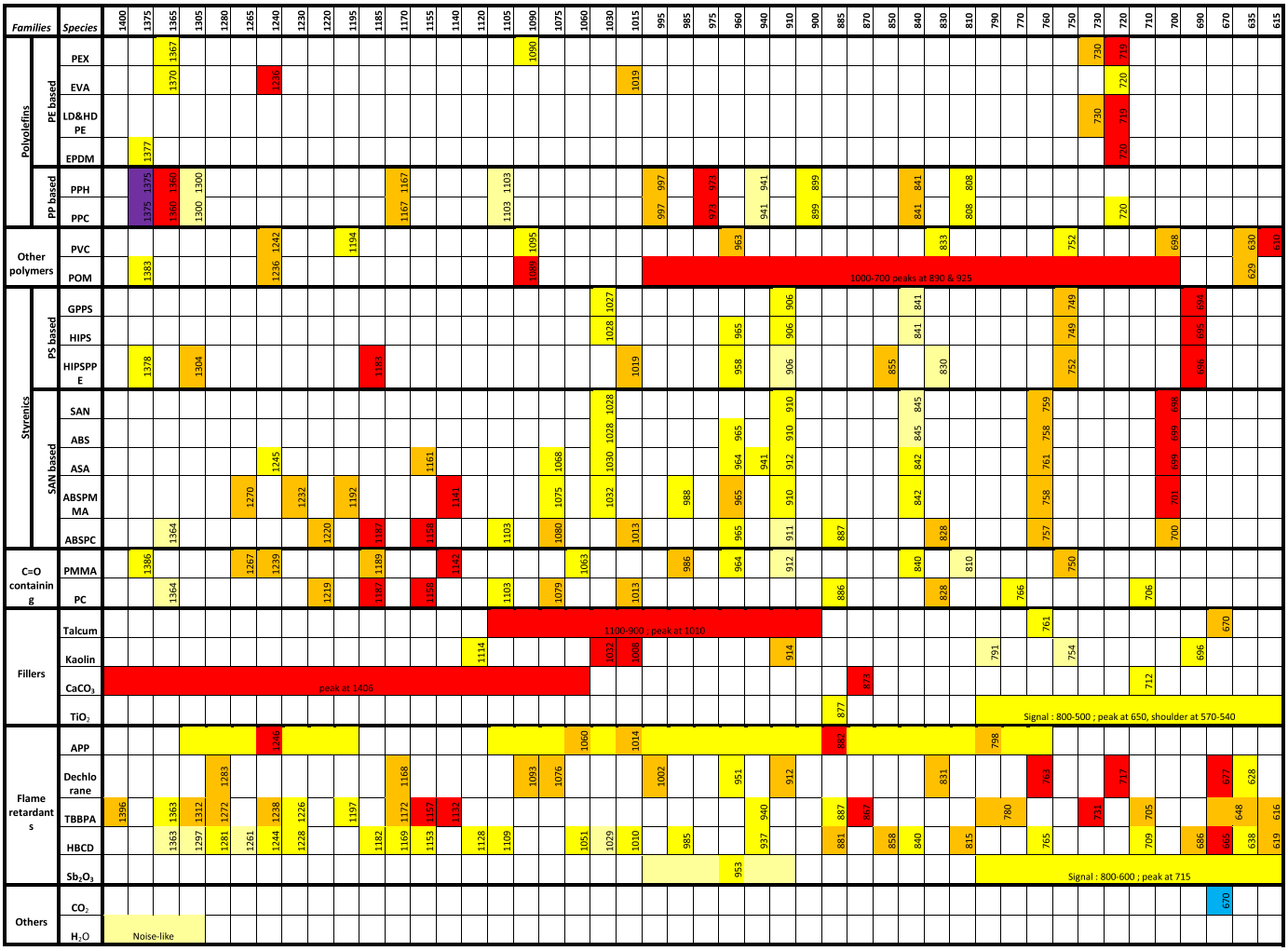

References

Aldrian, A., Ledersteger, A., Pomberger, R., 2015. Monitoring of WEEE plastics in regards to brominated flame retardants using handheld XRF. Waste Manag 36, 297–304. https://doi.org/10.1016/j.wasman.2014.10.025.

Allen, N.S., Edge, M., Corrales, T., Childs, A., Liauw, C.M., Catalina, F., Peinado, C., Minihan, A., Aldcroft, D., 1998. Ageing and stabilisation of filled polymers: an overview. Polym. Degrad. Stab. 61, 183–199. https://doi.org/10.1016/S0141-3910(97)00114-6.

Ashkiki, A.R., Felske, C., McCartney, D., 2019. Impacts of seasonal variation and operating parameters on double-stage trommel performance. Waste Manag 86, 36–48. https://doi.org/10.1016/j.wasman.2019.01.026.

Bae, J.-S., Oh, S.-K., Pedrycz, W., Fu, Z., 2019. Design of fuzzy radial basis function neural network classifier based on information data preprocessing for recycling black plastic wastes: comparative studies of ATR FT-IR and Raman spectroscopy. Appl. Intell. 49, 929–949. https://doi.org/10.1007/s10489-018-1300-5.

Barbier, S., Perrier, S., Freyermuth, P., Perrin, D., Gallard, B., Gilon, N., 2013. Plastic identification based on molecular and elemental information from laser induced breakdown spectra: a comparison of plasma conditions in view of efficient sorting. Spectrochim. Acta - Part B At. Spectrosc. 88, 167–173. https://doi.org/10.1016/j.sab.2013.06.007.

Becker, W., Sachsenheimer, K., Klemenz, M., 2017. Detection of black plastics in the middle infrared spectrum (MIR) using photon up-conversion technique for polymer recycling purposes. Polymers (Basel) 9, 435. https://doi.org/10.3390/polym9090435.

Beigbeder, J., Perrin, D., Mascaro, J.-F., Lopez-Cuesta, J.-M., 2013. Study of the physico-chemical properties of recycled polymers from waste electrical and electronic equipment (WEEE) sorted by high resolution near infrared devices. Resour. Conserv. Recycl. 78, 105–114. https://doi.org/10.1016/j.resconrec.2013.07.006.

Bokobza, L., Bruneel, J.L., Couzi, M., 2013. Raman spectroscopic investigation of carbon-based materials and their composites. Comparison between carbon nanotubes and carbon black. Chem. Phys. Lett. 590, 153–159. https://doi.org/10.1016/j.cplett.2013.10.071.

Delva, L., Hubo, S., Cardon, L., Ragaert, K., 2018. On the role of flame retardants in mechanical recycling of solid plastic waste. Waste Manag 82, 198–206. https://doi.org/10.1016/j.wasman.2018.10.030.

Fletcher, W.H., Rayside, J.S., 1974. High resolution vibrational Raman spectrum of oxygen. J. Raman Spectrosc. 2, 3–14. https://doi.org/10.1002/jrs.1250020102.

Florestan, J., Lachambre, A., Mermilliod, N., Boulou, J.C., Marfisi, C., 1994. Recycling of plastics: automatic identification of polymers by spectroscopic methods. Resour. Conserv. Recycl. 10, 67–74. https://doi.org/10.1016/0921-3449(94)90039-6.

Gallen, C., Banks, A., Brandsma, S., Baduel, C., Thai, P., Eaglesham, G., Heffernan, A., Leonards, P., Bainton, P., Mueller, J.F., 2014. Towards development of a rapid and effective non-destructive testing strategy to identify brominated flame retardants in the plastics of consumer products. Sci. Total Environ. 491–492, 255–265. https://doi.org/10.1016/j.scitotenv.2014.01.074.

Gent, M.R., Menendez, M., Toraño, J., Diego, I., 2009. Recycling of plastic waste by density separation: prospects for optimization. Waste Manag. Res. 27, 175–187. https://doi.org/10.1177/0734242X08096950.

Grause, G., Fonseca, J.D., Tanaka, H., Bhaskar, T., Kameda, T., Yoshioka, T., 2015. A novel process for the removal of bromine from styrene polymers containing brominated flame retardant. Polym. Degrad. Stab. 112, 86–93. https://doi.org/10.1016/j.polymdegradstab.2014.12.017.

Grégoire, S., Boudinet, M., Pelascini, F., Surma, F., Detalle, V., Holl, Y., 2011. Laser-induced breakdown spectroscopy for polymer identification. Anal. Bioanal. Chem. 400, 3331–3340. https://doi.org/10.1007/s00216-011-4898-2.

Gundupalli, S.P., Hait, S., Thakur, A., 2017. A review on automated sorting of source-separated municipal solid waste for recycling. Waste Manag 60, 56–74. https://doi.org/10.1016/j.wasman.2016.09.015.

Guzzonato, A., Mehlmann, H., Krumwiede, D., Harrad, S., 2016a. A novel method for quantification of decabromodiphenyl ether in plastics without sample preparation using direct insertion probe – magnetic sector high resolution mass spectrometry. Anal. Methods 8, 5487–5494. https://doi.org/10.1039/C6AY00460A.

Guzzonato, A., Puype, F., Harrad, S.J., 2016b. Improving the accuracy of hand-held X-ray fluorescence spectrometers as a tool for monitoring brominated flame retardants in waste polymers. Chemosphere 159, 89–95. https://doi.org/10.1016/J.CHEMOSPHERE.2016.05.086.
Hasan, A.R., Solo-Gabriele, H., Townsend, T., 2011. Online sorting of recovered wood waste by automated XRF-technology: Part II. Sorting efficiencies. Waste Manag. 31, 695–704. https://doi.org/10.1016/j.wasman.2010.10.024.
Hennebert, P., Filella, M., 2018. WEEE plastic sorting for bromine essential to enforce EU regulation. Waste Manag 71, 390–399. https://doi.org/10.1016/j.wasman.2017.09.031.
Hollas, J.M., 2004. Modern Spectroscopy, Fourth. ed. John Wiley & Sons, Ltd. Nature.
Hossain, M.Z., Yuan, Y., Teja, A.S., 2014. Measurement of enthalpies of association between CO2 and polymers via in situ ATR-FTIR spectroscopy. J. Supercrit. Fluids 95, 457–461. https://doi.org/10.1016/j.supflu.2014.10.018.
Huang, J., Tian, C., Ren, J., Bian, Z., 2017. Study on Impact Acoustic—Visual Sensor-Based Sorting of ELV Plastic Materials. Sensors 17, 1325. https://doi.org/10.3390/s17061325.
Huth-Fehre, T., Feldhoff, R., Kantimm, T., Quick, L., Winter, F., Cammann, K., Van Den Broek, W., Wienke, D., Melssen, W., Buydens, L., 1995. NIR - Remote sensing and artificial neural networks for rapid identification of Post Consumer Plastics. J. Mol. Struct. 348, 143–146. https://doi.org/10.1016/0022-2860(95)08609-Y.
Kang, M.-J., Heo, Y.-J., Jin, F.-L., Park, S.-J., 2016. A review: role of interfacial adhesion between carbon blacks and elastomeric materials. Carbon Lett 18, 1–10. https://doi.org/10.5714/CL.2016.18.001.
Kassouf, A., Maalouly, J., Rutledge, D.N., Chebib, H., Ducruet, V., 2014. Rapid discrimination of plastic packaging materials using MIR spectroscopy coupled with independent components analysis (ICA). Waste Manag 34, 2131–2138. https://doi.org/10.1016/j.wasman.2014.06.015.
Keeler, J., 2004. Lecture - Chapter 4 : Fourier transformation and data processing.
Krivtsova, G.B., Pimenov, A.N., Petukhov, V.V., 2009. Electromagnetic separation of nonferrous metals before a metallurgical conversion in a field of high-frequency current. Metallurgist 53, 524–530. https://doi.org/10.1007/s11015-009-9192-6.
Kuang, J., Abdallah, M.A.-E., Harrad, S., 2018. Brominated flame retardants in black plastic kitchen utensils: concentrations and human exposure implications. Sci. Total Environ. 610–611, 1138–1146. https://doi.org/10.1016/j.scitotenv.2017.08.173.
Küter, A., Reible, S., Geibig, T., Nüßler, D., Pohl, N., 2018. THz imaging for recycling of black plastics. tm - Tech. Mess. 85, 191–201. https://doi.org/10.1515/teme-2017-0062.
Langhals, H., Zgela, D., Schlücker, T., 2014. High performance recycling of polymers by means of their fluorescence lifetimes. Green Sustain. Chem. 04, 144–150. https://doi.org/10.4236/gsc.2014.43019.
Ledford, E.B., White, R.L., Ghaderi, S., Gross, M.L., Wilkins, C.L., 1980. Convolution-based phase correction in Fourier transform mass spectrometry. Anal. Chem. 52, 1090–1094. https://doi.org/10.1021/ac50057a022.
Leitner, R., Mairer, H., Kercek, A., 2003. Real-time classification of polymers with NIR spectral imaging and blob analysis. Real-Time Imaging 9, 245–251. https://doi.org/10.1016/j.rti.2003.09.016.
Li, Y., Huang, X., Zeng, L., Li, R., Tian, H., Fu, X., Wang, Y., Zhong, W.-H., 2019. A review of the electrical and mechanical properties of carbon nanofiller-reinforced polymer composites. J. Mater. Sci. 54, 1036–1076. https://doi.org/10.1007/s10853-018-3006-9.
Liu, M., Horrocks, A.., 2002. Effect of Carbon Black on UV stability of LLDPE films under artificial weathering conditions. Polym. Degrad. Stab. 75, 485–499. https://doi.org/10.1016/S0141-3910(01)00252-X.
Liu, X., Zhang, X., Zhang, K., Qi, C., 2016. Sodium persulfate-assisted mechanochemical degradation of tetrabromobisphenol A: efficacy, products and pathway. Chemosphere 150, 551–558. https://doi.org/10.1016/j.chemosphere.2015.08.055.
Ma, C., Yu, J., Wang, B., Song, Z., Xiang, J., Hu, S., Su, S., Sun, L., 2016. Chemical recycling of brominated flame retarded plastics from e-waste for clean fuels production: a review. Renew. Sustain. Energy Rev. 61, 433–450. https://doi.org/10.1016/j.rser.2016.04.020.
Maris, E., Botané, P., Wavrer, P., Froelich, D., 2015. Characterizing plastics originating from WEEE: A case study in France. Miner. Eng. 76, 28–37. https://doi.org/10.1016/j.mineng.2014.12.034.
Maris, J., Bourdon, S., Brossard, J.-M., Cauret, L., Fontaine, L., Montembault, V., 2018. Mechanical recycling: Compatibilization of mixed thermoplastic wastes. Polym. Degrad. Stab. 147, 245–266. https://doi.org/10.1016/j.polymdegradstab.2017.11.001.
Mazaheri, M., Johnson, G.R., Morawska, L., 2009. Application of bag sampling technique for particle size distribution measurements. J. Environ. Monit. 11, 2087. https://doi.org/10.1039/b907891f.
Mesina, M.B., de Jong, T.P.R., Dalmijn, W.L., 2007. Automatic sorting of scrap metals with a combined electromagnetic and dual energy X-ray transmission sensor. Int. J. Miner. Process. 82, 222–232. https://doi.org/10.1016/j.minpro.2006.10.006.
Otake, T., Itoh, N., Ohata, M., Hanari, N., 2015. Optimization of Microwave-Assisted Extraction for the Determination of Organic Flame Retardants in Acrylonitrile Butadiene Styrene. Anal. Lett. 48, 2319–2328. https://doi.org/10.1080/00032719.2015.1027898.
Peeters, J.R., Vanegas, P., Tange, L., Van Houwelingen, J., Duflou, J.R., 2014. Closed loop recycling of plastics containing Flame Retardants. Resour. Conserv. Recycl. 84, 35–43. https://doi.org/10.1016/j.resconrec.2013.12.006.
Probst, N., Van Bellingen, C., Van den Bergh, H., 2009. Compounding with conductive carbon black. Plast. Addit. Compd. 11, 24–27. https://doi.org/10.1016/S1464-391X(09)70080-7.
Puype, F., Ackerman, L.K., Samsonek, J., 2019. Evaluation of Direct Analysis in Real Time – High Resolution Mass Spectrometry (DART-HRMS) for WEEE specific substance determination in polymeric samples. Chemosphere 232, 481–488. https://doi.org/10.1016/j.chemosphere.2019.05.166.
Roh, S.-B., Oh, S.-K., Park, E.-K., Choi, W.Z., 2017. Identification of black plastics realized with the aid of Raman spectroscopy and fuzzy radial basis function neural networks classifier. J. Mater. Cycles Waste Manag. 19, 1093–1105. https://doi.org/10.1007/s10163-017-0620-6.
Rozenstein, O., Puckrin, E., Adamowski, J., 2017. Development of a new approach based on midwave infrared spectroscopy for post-consumer black plastic waste sorting in the recycling industry. Waste Manag 68, 38–44. https://doi.org/10.1016/j.wasman.2017.07.023.
Schlummer, M., Brandl, F., Mäurer, A., Van Eldik, R., 2005. Analysis of flame retardant additives in polymer fractions of waste of electric and electronic equipment (WEEE) by means of HPLC-UV/MS and GPC-HPLC-UV. J. Chromatogr. A 1064, 39–51. https://doi.org/10.1016/j.chroma.2004.12.016.
Serranti, S., Gargiulo, A., Bonifazi, G., 2012. Classification of polyolefins from building and construction waste using NIR hyperspectral imaging system. Resour. Conserv. Recycl. 61, 52–58. https://doi.org/10.1016/j.resconrec.2012.01.007.
Sharkey, M., Abdallah, M.A.-E., Drage, D.S., Harrad, S., Berresheim, H., 2018. Portable X-ray fluorescence for the detection of POP-BFRs in waste plastics. Sci. Total Environ. 639, 49–57. https://doi.org/10.1016/j.scitotenv.2018.05.132.
Signoret, C., Caro-Bretelle, A.-S., Lopez-Cuesta, J.-M., Ienny, P., Perrin, D., 2019a. MIR spectral characterization of plastic to enable discrimination in an industrial recycling context: I. Specific case of styrenic polymers. Waste Manag. 95, 513–525. https://doi.org/10.1016/j.wasman.2019.05.050.
Signoret, C., Caro-Bretelle, A.-S., Lopez-Cuesta, J.-M., Ienny, P., Perrin, D., 2019b. MIR spectral characterization of plastic to enable discrimination in an industrial recycling context: II. Specific case of polyolefins. Waste Manag. 98, 160–172. https://doi.org/10.1016/j.wasman.2019.08.010.
Signoret, C., Edo, M., Caro-Bretelle, A.-S., Lopez-Cuesta, J.-M., Ienny, P., Perrin, D., 2020. MIR spectral characterization of plastic to enable discrimination in an industrial recycling context: III. Anticipating impacts of ageing on identification. Waste Manag. 109, 51–64. https://doi.org/10.1016/j.wasman.2020.04.043.
Spetale, F.E., Bulacio, P., Guillaume, S., Murillo, J., Tapia, E., 2016. A spectral envelope approach towards effective SVM-RFE on infrared data. Pattern Recognit. Lett. 71, 59–65. https://doi.org/10.1016/j.patrec.2015.12.007.
Stenvall, E., Tostar, S., Boldizar, A., Foreman, M.R.S., Möller, K., 2013. An analysis of the composition and metal contamination of plastics from waste electrical and electronic equipment (WEEE). Waste Manag 33, 915–922. https://doi.org/10.1016/j.wasman.2012.12.022.
Szilasi, S.Z., Huszank, R., Szikra, D., Váczi, T., Rajta, I., Nagy, I., 2011. Chemical changes in PMMA as a function of depth due to proton beam irradiation. Mater. Chem. Phys. 130, 702–707. https://doi.org/10.1016/j.matchemphys.2011.07.048.
Tachwali, Y., Al-Assaf, Y., Al-Ali, A.R., 2007. Automatic multistage classification system for plastic bottles recycling. Resour. Conserv. Recycl. 52, 266–285. https://doi.org/10.1016/j.resconrec.2007.03.008.
Turner, A., 2018. Black plastics: linear and circular economies, hazardous additives and marine pollution. Environ. Int. 117, 308–318 https://doi.org/S0160412018302125.
van den Broek, W.H.A, Wienke, D., Melssen, W., Buydens, L.M., 1998. Plastic material identification with spectroscopic near infrared imaging and artificial neural networks. Anal. Chim. Acta 361, 161–176. https://doi.org/10.1016/S0003-2670(98)00012-9.
Vilaplana, F., Karlsson, P., Ribes-Greus, A., Ivarsson, P., Karlsson, S., 2008. Analysis of brominated flame retardants in styrenic polymers. J. Chromatogr. A 1196–1197, 139–146. https://doi.org/10.1016/j.chroma.2008.05.001.
Vilaplana, F., Ribes-Greus, A., Karlsson, S., 2009. Microwave-assisted extraction for qualitative and quantitative determination of brominated flame retardants in styrenic plastic fractions from waste electrical and electronic equipment (WEEE). Talanta 78, 33–39. https://doi.org/10.1016/j.talanta.2008.10.038.
Vrancken, C., Longhurst, P.J., Wagland, S.T., 2017. Critical review of real-time methods for solid waste characterisation: informing material recovery and fuel production. Waste Manag 61, 40–57. https://doi.org/10.1016/j.wasman.2017.01.019.
Wäger, P.A., Hischier, R., 2015. Life cycle assessment of post-consumer plastics production from waste electrical and electronic equipment (WEEE) treatment residues in a Central European plastics recycling plant. Sci. Total Environ. 529, 158–167. https://doi.org/10.1016/j.scitotenv.2015.05.043.
Wang, C., Wang, H., Fu, J., Liu, Y., 2015. Flotation separation of waste plastics for recycling—A review. Waste Manag 41, 28–38. https://doi.org/10.1016/j.wasman.2015.03.027.
WRAP, 2008. LCA of management options for mixed waste plastics. Waste resource action programme (WRAP).
Yamaji, Y., Okaya, K., Dodbiba, G., Wang, L.P., Fujita, T., 2013. A novel separation method for plastic of discarded appliance including black plastic by using Raman spectroscopy. Resour. Process. 60, 65–71. https://doi.org/10.4144/rpsj.60.65.
Yang, X., Sun, L., Xiang, J., Hu, S., Su, S., 2013. Pyrolysis and dehalogenation of plastics from waste electrical and electronic equipment (WEEE): A review. Waste Manag 33, 462–473. https://doi.org/10.1016/j.wasman.2012.07.025.
Zhao, P., Xie, J., Gu, F., Sharmin, N., Hall, P., Fu, J., 2018. Separation of mixed waste plastics via magnetic levitation. Waste Manag 76, 46–54. https://doi.org/10.1016/j.wasman.2018.02.051.
Zhao, Y.-B., Lv, X.-D., Ni, H.-G., 2018. Solvent-based separation and recycling of waste plastics: a review. Chemosphere 209, 707–720. https://doi.org/10.1016/j.chemosphere.2018.06.095.
Zhou, Z., Wang, S., Zhang, Yong, Zhang, Yinxi, 2006. Effect of different carbon fillers on the properties of PP composites: comparison of carbon black with multiwalled carbon nanotubes. J. Appl. Polym. Sci. 102, 4823–4830. https://doi.org/10.1002/app.24722.